MEASUREMENTS AND TEST OF METU OBSERVATORY SITE

A Master of Science Thesis

Presented by

Sinan Kaan YERLİ

to

the Graduate School of Natural and Applied Sciences

of Middle East Technical University

in Partial Fulfillment for the Degree of

MASTER OF SCIENCE

in

PHYSICS

MIDDLE EAST TECHNICAL UNIVERSITY

ANKARA

January, 1993

Approval of the Graduate School of Natural and Applied Sciences.

Prof. Alpay Ankara
Director

I certify that this thesis satisfies all the requirements as a thesis for the degree of Master of Science.

Prof. Şinasi Ellialıoğlu
Chairman of the Department

We certify that we have read this thesis and that in our opinion it is fully adequate, in scope and quality, as a thesis for the degree of Master of Science in Physics.

Prof. Ümit Kızıloğlu
Supervisor

Examining Committee in Charge:

Prof. Osman Demircan (Chairman) .....

Prof. Ümit Kızıloğlu .....

Y.Doç.Dr. Akif Esendemir .....

ABSTRACT

MEASUREMENTS AND TEST OF METU OBSERVATORY SITE

YERLİ, Sinan Kaan

M.S. in Physics

Supervisor: Prof. Ümit Kızıloğlu

January, 1993, 77 pages.

The METU Observatory site is tested for background light, light pollution and limiting magnitude. South direction in azimuth and altitude is found to be the clearest for the time being. By observing galactic clusters, limiting magnitude is found to be $10^{m}.16 \pm 0.13$ in V and $9^{m}.50 \pm 0.13$ in B filters. Geographic coordinates of the observatory site are found to be $32^{\circ}46'28''.2 \pm 1'09''.5$ in longitude, and $39^{\circ}54'10''.2 \pm 1'04''.1$ in latitude. Newly installed CCD (Charge Coupled Device) Camera is calibrated by using the flat-field images. Observing parameters of the instrument are calculated using the galactic cluster observations. Comet Swift-Tuttle is also observed with this instrument, and coma diameter and apparent velocity of the comet are calculated. The base for the future observations with this instrument is also prepared.

Key Words: Site Testing, Calibration, Photometry, CCD

Science Code: 402.02.01

ÖZ

ODTÜ GÖZLEMEVİ BÖLGESİNİN TEST VE ÖLÇÜMLERİ

YERLİ, Sinan Kaan

Yüksek Lisans Tezi, Fizik Anabilim Dalı

Tez Yöneticisi: Prof. Ümit Kızıloğlu

Ocak, 1993, 77 sayfa.

ODTÜ Gözlemevi bölgesi, arka ışık, ışık kirlenmesi ve kadir sınırı için test edildi. Azimut ve yükseklik için Güney yönü, şu an için en temiz olarak bulundu. Gökada kümeleri gözlenerek, kadir sınırı V filitresinde $10^{m}.16 \pm 0.13$, B filitresinde $9^{m}.50 \pm 0.13$ olarak bulundu. Gözlemevi bölgesinin coğrafik konumu $32^{o}46'28''.2 \pm 1'09''.5$ doğu boylamı, ve $39^{o}54'10''.2 \pm 1'04''.1$ kuzey enlemi olarak bulundu. Yeni kurulan CCD (Yük-Biriktirmeli-Aktarmalı Algılayıcı) kamera düz-alan görüntüleri yardımıyla ayarlandı. Aletin gözlemsel parametreleri, gökada kümeleri gözlemleriyle hesaplandı. Bu aletle kuyrukluyıldız Swift-Tuttle gözlendi, ve kuyrukluyıldızın koma çapı ve görünür hızı da hesaplandı. Bu aletle, ileride yapılacak gözlemler için bir taban da oluşturulmuştur.

Anahtar Kelimeler: Bölge Testi, Kalibrasyon, Fotometre, CCD

Bilim Dalı Sayısal Kodu: 402.02.01

ACKNOWLEDGEMENTS

I would like to thank to Prof. Ümit Kızıloğlu for his discussions, throughout the course of this work.

My thanks are also due to my wife Çiçek Öztek, for her encouragement and assistance in the observations.

I would like to thank also to my friends İsmail Ergün, Cem Özen and Enis Tuncer for their assistances in the observations.

I am very happy to thank also to every astronomer and astrophysicist in Turkey for their valuable performance which make the subjects functioning.

TABLE OF CONTENTS

LIST OF TABLES

LIST OF FIGURES

CHAPTER I

INTRODUCTION

An observatory, in a common sense, is a building containing a considerably big telescope, with necessary instruments for observation in the optical part of the spectrum. However in observatories, built for universities, there are educational subjects for preparing new astronomers by showing the experimental side of the astronomy and astrophysics.

It is not a rule but it is logical that, when constructing an observatory, first a site with convenient requirements must be selected and then instrumentation and their calibrations must be carried out. However, METU observatory, due to difficulties in building far from the campus, had been built in it (but away from the departments and in a small valley to prevent the site from the city light). Now we are carrying out test, measurements of the site and calibration of the instruments. This much of distance (1.5km away from the departments) was enough in 1986. Now, however, the new buildings are being constructed near to the observatory.

The construction of the main building of the observatory was started in 1986-1987 and it was completed in 1989. The telescope was bought from USA in 1975 and installed to the pillar in 1990. Between 1975 and 1990, it was used in a small housing near to the physics building. In September 1990, the opening made and observations were started next summer in 1991.

In this work, the main subject was to find limits of the site and instruments. Standard measurements for a site are not accomplished in this work. By making a complete site testing, one can obtain more precise values by using quite a large number of observations, however, the same values can be approximated by a limited observations.

Thus throughout this work, all measurements and tests have meanings of 'in which order of magnitudes can we do observations with the installed instruments'.

Since light pollution is the major destructive effect for the site, limiting magnitude determination will be helpful on planning an observing program. Such a limit can be achieved by first surveying major directions of the light pollution and then measuring the limiting magnitude of the site with the instrumentation used frequently. Surveying is done successfully by a photomultiplier tube (PMT) with a pointer and limiting magnitudes are found for Johnson's V and B filters attached to a SSP-3 photometer by monitoring some galactic clusters.

Surveying of the sky for the light pollution is carried out in eleven nights during 1991 and 1992. Before starting the observations, PMT is tested for scaling and high voltage adjustment. Finally 1200V and 10μA are chosen to be the proper measurement values for the PMT. All the observations are then carried out with these values and at the same place for a comparison. To normalize all the observations, zenith is taken to be the reference point, where the light pollution and the air-mass have minimum values.

Limiting magnitude is calculated using three galactic clusters: Praesepe (NGC 2632), Coma Cluster (Mel 111) and NGC 6633. All of the selected stars have spectral types of A (except one F0V). Stars are selected according to their (B-V) values, and keeping in mind the observing limit of the SSP-3 photometer. Limiting magnitude is determined by comparing observed raw instrumental magnitudes with the assigned standard magnitudes of the stars. This is done for both Johnson filters of V and B.

Geographic coordinates of the site are measured using a theodolite. In this work the observations of α Aquila are carried out for five nights.

Newly installed CCD (Charge Coupled Device) camera, is also calibrated using flat-field observations. NGC6633 is also observed with CCD, to adjust the system settings properly. Comet Swift-Tuttle is also observed for one night. Some more introductory images by the CCD camera consisting of Moon, Saturn, and M13 were also obtained.

CHAPTER II

MAIN SITE MEASUREMENTS & TESTS

2.1 Determination of Geographic Coordinates of the Observatory Site

2.1.1 Methods for finding longitude and latitude

In finding geographic coordinates of a site there are so many methods with accuracies ranging from arcseconds to arcminutes. Some basic methods are listed below and explained briefly:

Latitude

When a star is on the meridian

$$\phi = \delta \pm z \tag{2.1}$$

where ϕ is the geographic latitude, δ the declination of the star, and z is the zenith angle of the star. The sign is positive when the star is south of the pole and remember that the south declinations are negative.

1. *Meridian altitudes:* The simplest observation. In this method equation 2.1 is used when a star transits in the meridian and a single maximum altitude is obtained. One can observe more stars, to reduce the error in declination. Care should be taken in choosing the stars; maximum altitude of the star should be greater than 30^o and the declination of the star should be less than 88^o. Accuracy is around the standard error of $1''$.

2. *Circum-meridian altitudes:* In this method observations are continued before and after the transit and corrected to give the value of z on the meridian. For this

method maximum altitude of the stars should be in between 30° and 70°. Pairs should be within 5°. With a programme of three north and three south stars, apparent standard error will be less than 1″.

3. *Talcott Method or Horrebow-Talcott Method:* In this method a zenith telescope is used in the observations. In the observing programme, there are two stars, having declinations of δ_1 and δ_2, and they transit at the zenith distances of z and $z + \delta z$ north and south of the zenith, respectively. Thus equation 2.1 gives

$$\phi = \frac{1}{2}(\delta_1 + \delta_2) + \frac{1}{2}\delta z \tag{2.2}$$

So z need not to be measured. The accuracy of the method with eight pairs of stars will probably give an standard error of 0″.5.

Longitude

$$\lambda = LMST - GMST \tag{2.3}$$

where $LMST$ is the local mean sideral time at which a star is at a certain altitude or azimuth at the site concerned, and the $GMST$ is the Greenwich mean sideral time at the same instant. Using simple time formulae, longitude can be calculated easily by obtaining the time of the transit of a star or pair of stars.

1. *Meridian Transits:* Meridian transit observation depends on the simple principle that the local apparent sideral time of a star's transit equals to its right ascension (RA) or its RA+12^h, if the transit is below the horizon. For this method traditionally, transit telescope or Danjon astrolabe is used. However, it can be done by using a theodolite, also.

2. *Zenith photography:* This method is used for measuring latitude and time with accuracies of $0''.01$ and $0^s.001$, respectively. The Photo-Zenith-Tubes are used in photography. Light from the lens is reflected from a mercury bath back to a small photographic plate just below the lens. With a focal length of 3.5m maximum meridian zenith distance is 15'. As the star transits, plate is moved at a constant speed, such that the image is stationary. For $9^m.5$ magnitude star 20 seconds of exposure is required. The clock seconds of time is recorded when the plate traversed. The construction of such instruments are so important than making the observations.

The methods listed above are due to Bomford, 1971.

2.1.2 The method used in this work

The following formulae are used for the calculations:

Longitude

$$\begin{aligned} \lambda &= LMST - GMST \\ &= LAST - GAST \\ &= \alpha_* - (GMST - EE) \end{aligned} \tag{2.4}$$

$$GMST = 6.5947030 + 0.0657098243 * d + 1.002273791 * t \quad 1992 \tag{2.5}$$

$$= 6.6106172 + 0.0657098243 * d + 1.002273791 * t \quad 1991$$

$$UT1 = LT \pm ZT$$

$$EE = \Delta\lambda + \cos(\epsilon) \tag{2.6}$$

where $LAST$ is equal to α_* (right ascension of the star), when the star is in transit, d is the day of the year, and t is the time of the transit in UT. ZT for Turkey is -2^h. EE is the equation of equinoxes, $\Delta\lambda$ is the nutation in longitude which is defined as the longitude of the mean vernal equinox relative to the true vernal equinoxes, and ϵ is the obliquity of the ecliptic:

$$
\begin{aligned}
l &= 218^\circ.316 + 481\,267^\circ.881 * T \\
m &= 134^\circ.963 + 477\,198^\circ.867 * T \\
\Omega &= 125^\circ.045 - \ 1\,934^\circ.136 * T \\
L &= 280^\circ.466 + \ 36\,000^\circ.770 * T \\
M &= 357^\circ.528 + \ 35\,999^\circ.050 * T \\
T &= (JD - 245\,1545.0)/26525
\end{aligned}
$$

$$
\begin{aligned}
\Delta\lambda &= -17''.200 * \sin(\Omega) + 0''.206 * \sin(2\Omega) \\
&\quad - 1''.319 * \sin(2L) + 0''.143 * \sin(M) \\
&\quad - 0''.227 * \sin(2l) + 0''.071 * \sin(m) \qquad (2.7) \\
\epsilon &= 23^\circ.439291 - 0^\circ.013004 * T \qquad (2.8)
\end{aligned}
$$

where JD is the Julian date of the transit time, l is the mean longitude of the moon, m is the mean anomaly of the moon, Ω is the mean longitude of the lunar node, L is the mean longitude of the sun, M is the mean anomaly of the sun.

Latitude

$$\phi = \delta_* \pm z$$

Table 2.1. Specifications of Nikon NT-4D theodolite

Magnification	30 x
Field of view	1°24'
Minimum increments	6".
Sensitivity of Plate level	30"/2mm

$$R = 0^{\circ}.00452 \times \frac{P}{T} \times \tan z \tag{2.9}$$

where ϕ is the latitude of the site, δ_* is the declination of the star, z is the observed zenith angle of the star, R is the correction for refraction with P (pressure) in millibars, T (temperature) in Kelvin's.

Formulae are due to the Astronomical Almanac of the years 1991 and 1992; Montebruck, 1989; and Aoki et.al 1982.

2.1.3 Observations

In this work Nikon NT-4D theodolite is used. Specifications of the theodolite is listed in table 2.1. Leveling is done with a bubble, leveling error of 30″/2mm. For every night this reading was maintained in $\leq$2mm range. Since the bubble correction is within the error of the bubble adjusted in a night, no bubble corrections is done not to lose much time in leveling the theodolite.

Five nights of observations are done in this work. Each night was clear, there were no clouds or haze. Each night the same star is observed. Specifications of the star is listed in table 2.2.

For each observation time (in UT) and zenith angle read from the theodolite, are recorded to an order of seconds and seconds of arc respectively. In recording time or reading the angle the mean errors were 1s and 3″, respectively. Time is calibrated using short wave radio signals, for each night.

Table 2.2. Specifications of α Aquila

Name	α Aquila, Altair, HD 187642
α	$19^h50^m46\overset{s}{.}8$ (Epoch 2000.0)
δ	$+8°52'06''$ (Epoch 2000.0)
m_V	$0\overset{m}{.}77$
Spectral Type	A7IV-V

Program of the observation is as follows:

- Before meridian transit, observation was started.
- In 3-5 minutes of time zenith angle and the time was recorded when the star was exactly on the cross-hair of the theodolite.
- Near the transit, positioning the cross-hair onto the star was difficult and erroneous, so 1-2 minutes before the expected time of transit, observations switched from 'reading the zenith angle' to 'setting the zenith angle at the theodolite'.
- From now on, last recorded zenith angle was set at the theodolite and waited until the star was on the cross-hair. At the time of intersection, the time was recorded.
- This procedure continued until the first recorded zenith angle.

2.1.4 Results

For each night a second degree, polynomial fit is applied to find the minimum zenith distance and time of transit (figure 2.1). The results of the fits and calculated λ and ϕ values are listed in table 2.3. α and δ of the star is corrected for proper motion. Also observed zenith distances are corrected for the refraction using the equation 2.9. All the necessary corrections or used values are listed in table 2.4.

Table 2.3. Results of the transit observations and calculated λ and ϕ values from the 2^{nd} order fits applied to the observations

Date	t_0	z_0	GAST	λ	ϕ
12/08/92	$20^h13^m15^s.08$	$31°03'16''.24$	$17^h39^m20^s.54$	$32°46'17''.28$	$39°54'14''.36$
17/08/92	$19^h53^m36^s.32$	$31°03'54''.89$	$17^h39^m21^s.29$	$32°46'06''.68$	$39°54'53''.14$
18/08/92	$19^h49^m37^s.82$	$31°03'22''.08$	$17^h39^m18^s.69$	$32°46'45''.84$	$39°54'20''.35$
19/08/92	$19^h45^m43^s.12$	$31°02'32''.69$	$17^h39^m19^s.90$	$32°46'27''.91$	$39°53'30''.99$
20/08/92	$19^h41^m46^s.19$	$31°02'53''.56$	$17^h39^m18^s.88$	$32°46'43''.36$	$39°53'51''.88$

Table 2.4. Proper motion of the star and pressure and tempature of the observation nights

Date	α_{date}	δ_{date}	P_{sea}(mbar)	T(°K)
12/08/92	$19^h50^m25^s.69$	$+8°50'58''.12$	1009.7	298.4
17/08/92	$19^h50^m25^s.74$	$+8°50'58''.25$	1009.3	297.8
18/08/92	$19^h50^m25^s.75$	$+8°50'58''.27$	1011.1	290.0
19/08/92	$19^h50^m25^s.76$	$+8°50'58''.30$	1013.6	296.2
20/08/92	$19^h50^m25^s.77$	$+8°50'58''.32$	1009.5	298.8

Pressure and temperature values are obtained from the Meteorological General Directory. Temperature values are for the time of 21^h. Pressure values are converted to the sea level.

Final values of λ and ϕ, and their mean errors are as follows:

$$\lambda = 32°46'28''.2 \pm 1'09''.5 \quad (2.10)$$

$$\phi = 39°54'10''.2 \pm 1'04''.1 \quad (2.11)$$

These values can be compared with the values calculated by Yaşar (1991) for a site near to the observatory, and with the values of Ankara University, Ahlatlıbel Observatory (The Astronomical Almanac, 1992). Distance between Ahlatlıbel and METU Observatory is approximately 5600 meters taken from the university map (1:10000) which makes 3'.0 arcminutes, very close to the calculated difference 3'.6.

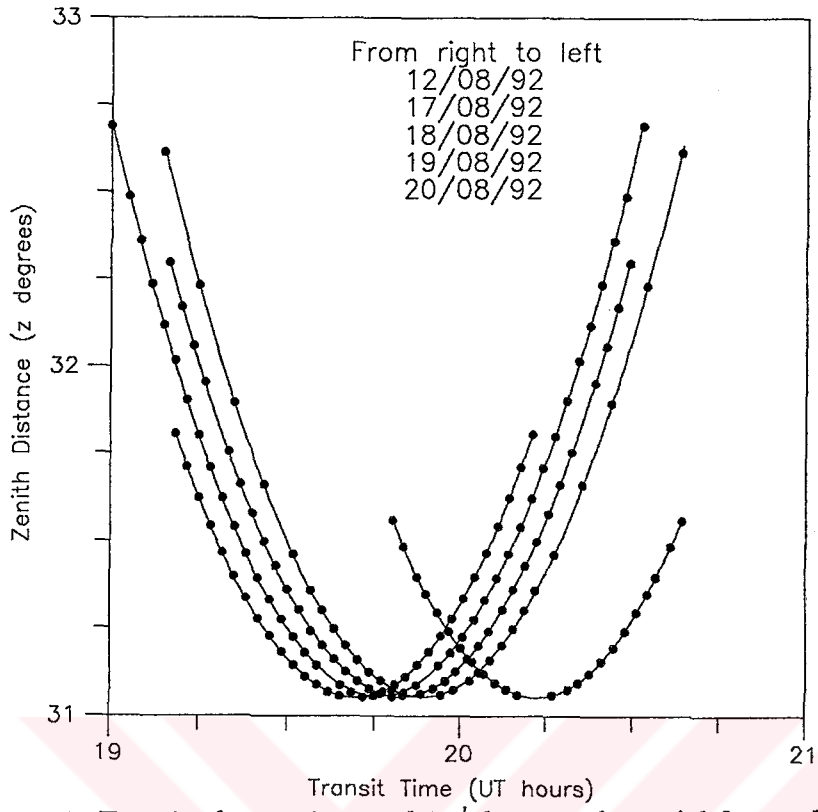

Figure 2.1. Transit observations and 2^{nd} degree polynomial fits applied to them

	λ	ϕ
Yasar, 1991	32°47′37.″65	39°53′06.″09
Ahlatlıbel, 1992	32°46′48″	39°50′36″

There are also some more corrections for the observed and calculated values, however they are so small that they vanish in the mean error of the theodolite leveling.

2.2 Survey on the Background Light of the Site

2.2.1 Theory and Instrumentation

The observatory is built near to the city. So, background light of the site is considerably high. Thus observations should be done, with the knowledge of the background light at different regions of the sky. This can be obtained by surveying the

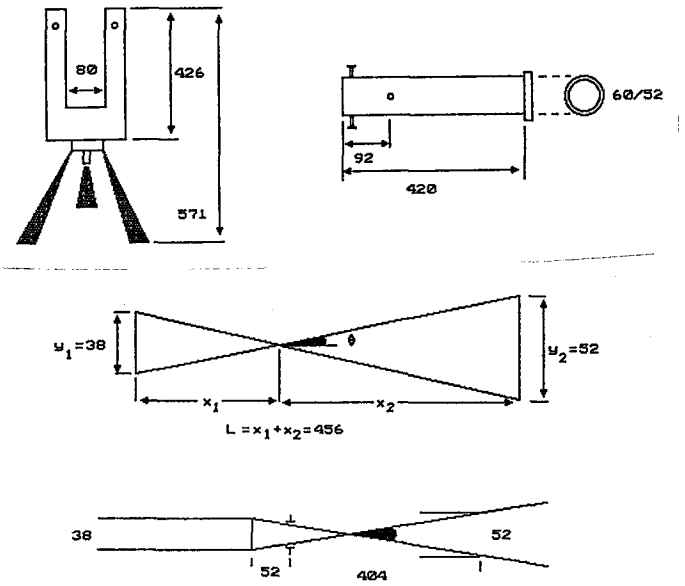

Figure 2.2. Schematic drawings of the sky pointer (top), dimensions of the buffle (middle) and measurements for the field of view (bottom)

sky for background light. In this work this is done by using a photomultiplier (PMT) tube and a pointer. Schematic drawings are shown in figure 2.2.

RCA-C70114F is used for PMT. Some typical characterizations of the tube are listed in table 2.5. Calculation of voltage divider chain is as follows; expecting 1500 volt maximum cathode-anode voltage and using 100K chain resistors, we should have 1.3 mA current in the PMT. Thus the average current that would be produced by the PMT, can be calculated by using following equation.

$$\bar{i} = \rho \times Area \times (Q)_\lambda \times Gain \times q \qquad (2.12)$$

where roughly $\rho = 10^7$ photon/cm^2/sec (Allen 1973), area of the tube is 11.4 cm^2, quantum efficiency (Q_λ) 0.25, gain or the current amplification of the tube is 0.5×10^6,

Table 2.5. Characterizations of RCA-C70114F

Spectral Response	# 115
Wavelength of Maximum Response	4000± 500Å
Cathode Semitransparent	Bialkali
Shape	Flat, Circular
Minimum Area	1.2 in^2
Minimum Diameter	1.24″
DC Supply Voltage	
Between Anode-Cathode	1800 max. volts
Between consecutive dynodes	300 max. volts
Average Anode Current	0.5 max. mA
Ambient Temperature Range	-100° to +85° C

Table 2.6. Field Test of the PMT and the pointer

Settings		Current	
C-A Voltage	Reading Scale	Zenith	Horizon (min-max)
1000 V	10 μA	0.16	1.0 - 5.0
1100 V	10 μA	0.30	2.0 - 12.0

electron charge (q) is 1.6×10^{-19}. Thus the average current would be 2.3 μA for minimum dark current. For safety it is taken as 23 μA. And when a blue light applied to the tube, a typical value of 50 μA can be obtained. Thus the average expected current when the tube is pointed to the sky would be 23×50 μA= 1.2 mA.

Field test is done on July 31, 1992. Night was exactly clear. Light pollution was accumulated in the direction of east and north-east. Also air pollution was in the same direction. Moon was setting in the direction of south-west. The test results are listed in table 2.6.

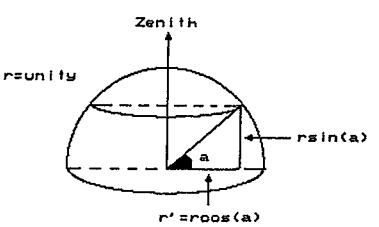

Figure 2.3. Schematic drawing of dividing the semi-sphere into altitude layers

Field of view calculations are done according to the final shape of the pointer. The dimensions of the buffle of the pointer are also shown in figure 2.2. All values are in mm. Using simple geometric equations x_1 and x_2 which are shown in figure 2.2, are calculated as 192.5 mm and 263.5 mm, respectively. Using equations 2.13 and 2.14, field of view in degrees (α) and in steradian (s) are found to be 11°.27 and 0.12, respectively, where θ, x_2, and y_2 are also shown in figure 2.2.

$$\alpha = 2\theta$$

$$\tan\theta = \frac{y_2/2}{x_2} \tag{2.13}$$

$$s = \frac{\pi R^2}{d^2} = \frac{\pi y_2^2}{x_2^2} \tag{2.14}$$

Surveying is done by dividing the sky into successive regions according to field of view. Not to have overlapped regions, pointing regions are taken as 15° wide. Number of regions to be observed at a given altitude is calculated by using simple sphere geometry (figure 2.3): $C = 2\pi x = 2\pi r \cos a$, where C is the circumference of the sphere layer at an altitude of a. Taking radius as unity, and scaling this circumference to the field of view, we would obtain the simple relation between number of regions at a given altitude as $\# = 24\cos a$. The overall sky scan is shown in table 2.7, where N_a is the number of observation points in altitude and N_A is the number of observation

Table 2.7. Pointing directions of the pointer for the calculated field of view

Altitude	N_a		Azimuth		N_A
90°	1.00 →	1	360° →	360°	1
75°	6.21 →	6	60° →	60°	6
60°	12.00 →	12	30° →	30°	12
45°	16.97 →	17	21° →	20°	18
30°	20.78 →	21	17° →	15°	24
15°	23.18 →	23	16° →	15°	24
0°	24.00 →	24	15° →	15°	24
		104			109

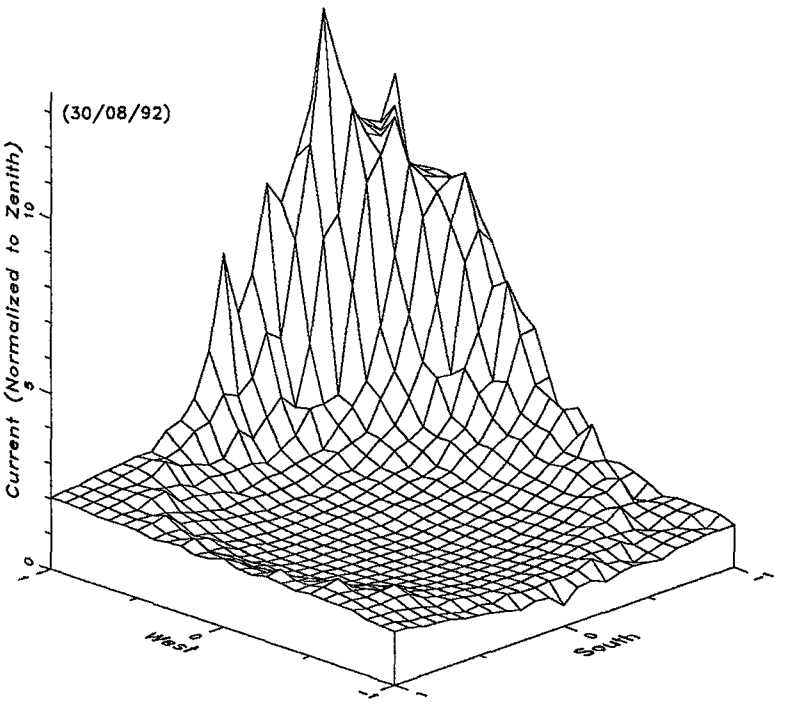

Figure 2.4. Surface plotting of the night August 30, 1992 which shows projected and normalized (to zenith) current values read from the pointer with respect to the pointing direction. High current values are the measure of the light pollution.

points in azimuth.

2.2.2 Observations

On five nights in 1991 and six nights 1992, totally on eleven nights, survey was carried out at the roof of the observatory. All the survey data were taken from the same place of the roof and with the same settings of the PMT and ampermeter. Reading scale of the ampermeter and cathode-anode voltage of the PMT is maintained at 10μA and 1200V, respectively for all the nights. Ten minutes of warming interval was performed by pointing to zenith before starting the sequence. Since the sky sweeps 15^o in a hour, surveying sequence had to be carried out in 40^m=2400^s to not to lose

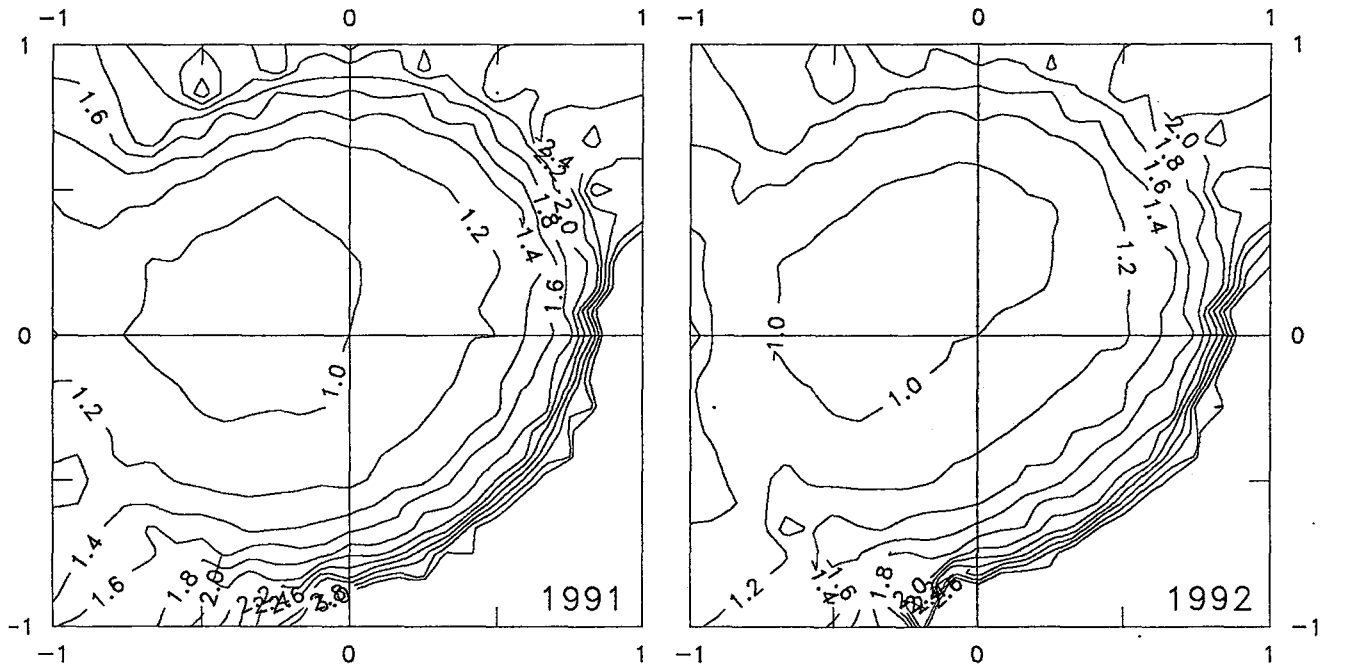

Figure 2.5. Topographical plots of normalized (w.r.t. zenith readings) observations, averaged for the years 1991 and 1992. North is to the right, East is to the bottom

a 15° region around the horizon. Totally 109 regions of the sky had to be observed; allowing 11^s for each region. Thus 5-7^s of integration time was chosen for safety.

Eleven observations are recorded with the information of altitude, azimuth and the current value, read from the ampermeter. The data then normalized to the zenith current value. For every night, projection of the altitude and the azimuth are performed to have X-Y-Z plot. Projection is calculated using following equtions;

$$x = \cos(altitude) * \cos(-azimuth) \tag{2.15}$$

$$y = \cos(altitude) * \sin(-azimuth) \tag{2.16}$$

A normalized sample graph for August 30, 1992 night data is shown on figure 2.4. Also topographical plots of yearly averages are shown in figure 2.5. As can be seen on the

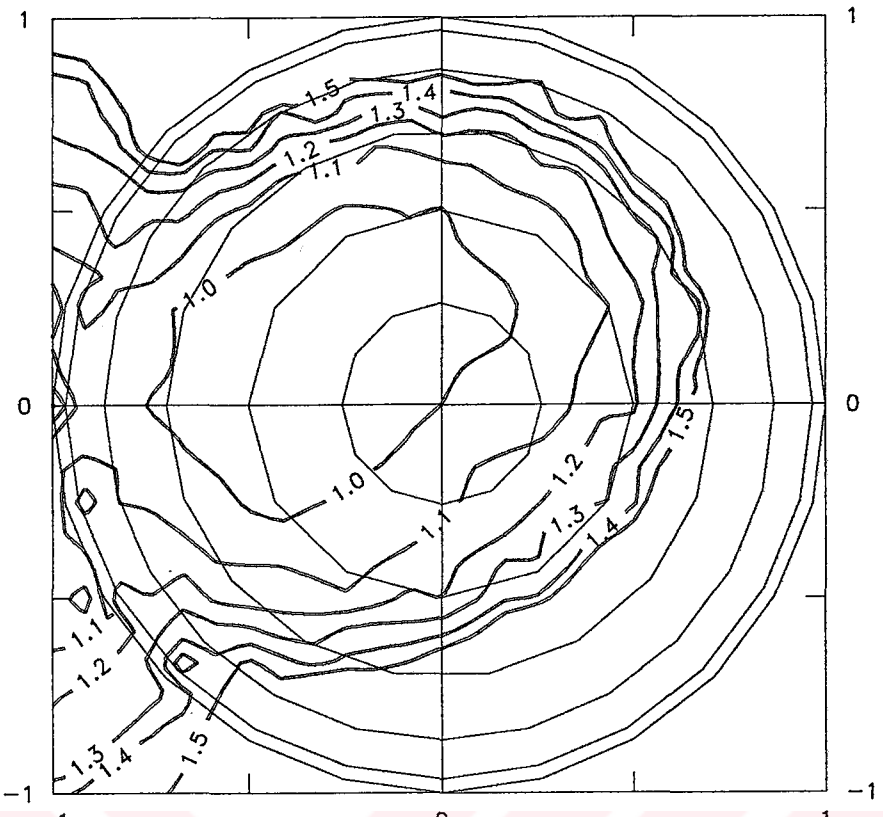

Figure 2.6. Topographical plot of the average of all of the normalized observations. Contour lines are 15° wide. North is to the right, East is to the bottom.

plots, contour lines in 1991, are spread in the direction of south and south west in 1992, which means that these directions are brighter in 1992 than in 1991. Also north, north-west and east directions show step trend to upper ratios in 1992, than in 1991.

Analysis of the average of all nights (from the figure 2.6) is shown in table 2.8. Where a is the altitude, A is the azimuth (min-max) and C_a $((max - min)/2)$ is the central azimuth of the given altitude for the current values from 1.0 to 1.5. Current values are converted to raw instrumental magnitude, using the fact that the current ratio of zenith and another reading is the same relation if you consider sky and star readings from a chart recorder.

Values show that the least light pollution is approximately on the south direction (180°) in azimuth and greater than 45° in altitude. Lower than 45° in altitude,

Table 2.8. Altitude, azimuth (min-max) and the central azimuth of the contour intervals between normalized values 1.0 and 1.5 of the average of all nights

	$\Delta m=0^m.00$		$\Delta m=0^m.10$		$\Delta m=0^m.20$		$\Delta m=0^m.28$		$\Delta m=0^m.37$		$\Delta m=0^m.44$	
a	A	C_a	A	C_a	A	C_a	A	C_a	A	C_a	A	C_a
90	360-360	360	-		-		-		-		-	
75	120-300	210	0-60	30	-		-		-		-	
60	150-300	225	120-330	225	0-90	45	30-60	45	-		-	
45	160-220	190	140-280	210	120-320	220	135-240	188	340-340	340	0-100	50
30	-		165-210	188	150-225	188	-		270-285	278	300-300	300
15	-		-		180-195	188	165-165	165	150-210	180	-	
0	165-165	165	135-210	173	-		120-255	188	-		-	

with a magnitude difference of $0^m.44$, again south (180°) direction is found. In between zenith and 45°, however, there are two separate windows. One is directed to south-west (220°), and the other one to north-east (40°). Practically, sky regions 90°-45° in altitude and 160°-240° in azimuth, can be monitored away from light pollution. Since all these observations depends on the strength of light pollution, on each year this surveying must be repeated.

2.3 Limiting Magnitude Estimation

In finding the limiting magnitude of the site with the installed instrumentation explained in appendix A, the method explained in section B.4 is taken as a base. A general introduction to the observational astronomy and its common observational methods are also discussed in appendix B. To estimate the limiting magnitude, standard stars of the galactic star clusters are used. In table 2.9, observed clusters and their parameters are given.

Type of the cluster is according to Trumpler (1930) which characterize the cluster's degree of concentration, range of its stars, and the richness in the following manner:

- *Concentration*

  I. Detached; strong concentration toward center.

  II. Detached; weak concentration toward center.

  III. Detached; no concentration toward center.

  IV. Not well detached from surrounding star field.

- *Range in brightness*

  1. Small range in brightness.

  2. Moderate range in brightness.

  3. Large range in brightness.

- *Richness*

  p. Poor (less than 50 stars).

  m. Moderately rich (50 to 100 stars).

  r. Rich (more than 100 stars).

Magnitude of the cluster is according to Skiff (1983). It is the cluster's total apparent V magnitude from UBV photometry. Age is in million years.

Three clusters on nine nights, totally 22 cycles of observations were done. All nights were photometric. Nights were chosen according to cloudless of the sky

Table 2.9. Observed galactic star clusters and their parameters

Name	Const.	Diam.	Type	Mag.	Spec.	Age
NGC 2632 (Praesepe)	Cnc	95'	II 2 m	$3^m.1$	A0	660
Mel 111 (Coma Cluster)	Com	275'	II 3 p	$1^m.8$	A0	400
NGC 6633	Oph	27'	III 2 m	$4^m.6$	B6	660

during the night. There were no haze, no cloud passages during the nights. Nights were also moonless. All the observations were done after the twilight was passed at least half an hour. All the electronics and the dome were stabilized by at least one hour. Between star passages, minimum telescope motion was arranged to eliminate the noise generated by the motors. Schedule of the observations is listed in table 2.10. All the observations were done with the SSP-3 photometer, except eight cycle of NGC 6633 on the 03/08/92 night. They were taken with Astro-Link CCD camera. Δ T is the total observation time and N is the total number of observed stars in the cluster.

Table 2.10. Schedule of the cluster observations

Date	Cluster	Δ T	N	Cycle(s)
02/05/92	NGC 2632	126	12	1
29/05/92	Mel 111	80	9	1
26/06/92	Mel 111	76	9	1
07/07/92	NGC 6633	46	5	2
24/07/92	NGC 6633	59	5	3
31/07/92	NGC 6633	104	5	5
02/08/92	NGC 6633	91	5	5
03/08/92	NGC 6633	32	5	2
03/08/92	NGC 6633	24	7	8

A cycle consist of sequential V and B deflections of selected stars from the cluster. Star deflections were squeezed by the sky deflections in both filter and time is extrapolated at the star deflection when filter is changed. Approximately 30 seconds of deflections were recorded using a chart recorder. Amplifier gain maintained constant during the cycle. However in wide magnitude ranges it was increased from a lower gain to a higher one. Time is taken in UT and it is arranged with a time unit which was synchronized with short wave radio signal. All the observations are listed in appendix C with tables C.1, C.2 and C.3 for each cluster.

Cluster stars are chosen according to their magnitude and cluster membership. Cluster membership is checked from V versus (B-V) graph of the cluster (figure 2.10. If star(s) thought to be a member of the cluster, they should be in the main sequence, where it is a band in the plot. Only the fourth star of the cluster NGC6633 have a shift in the main sequence. References for the graphs are as follows: *NGC 2632* Johnson (1952), *Mel 111* Johnson and Knuckles (1955), *NGC 6633* Hiltner et.al (1957). All the observed stars are listed in table 2.11. No, m_v, (B-V) and Spectral type data are taken from the references. A sequential number is assigned to each star for convenience and gain is arranged linearly.

Table 2.11. Stars observed in the clusters and their parameters

Cluster	#	No.	m_v	(B-V)	Spec.	Gain
NGC2632	8	224	$7^m.32$	0.19	A	5.0
	9	229	$7^m.54$	0.25	A	5.0
	11	265	$6^m.61$	0.01	A1 V	5.0
	12	276	$7^m.54$	0.16	A	5.0
	14	279	$7^m.70$	0.20	A	5.0
	16	286	$8^m.02$	0.19	A	5.0
	17	300	$6^m.30$	0.17	A6 III	2.5
	19	328	$6^m.85$	0.20	A9 III	5.0
	20	348	$6^m.78$	0.17	A6 V	5.0
Mel 111	7	104	$6^m.72$	0.24	A	5.0
	9	109	$6^m.40$	0.27	F0 V	5.0
	11	130	$4^m.99$	0.08	A4	1.0
	12	139	$6^m.73$	0.16	A	5.0
	13	144	$6^m.53$	0.18	A	5.0
	14	145	$6^m.63$	0.22	A	5.0
NGC6633	1	31	$8^m.77$	0.22		5.0
	2	32	$7^m.57$	0.02		5.0
	3	33	$8^m.26$	0.24		5.0
	4	56	$8^m.21$	0.82		5.0
	5	66	$8^m.18$	0.03		5.0

Main subject is to find the limiting magnitude for SSP-3 with V and B filters. All Δ deflections are measured between star and sky means. For each deflection pair of V and B, an airmass calculation is carried out using equation B.7. The deflections

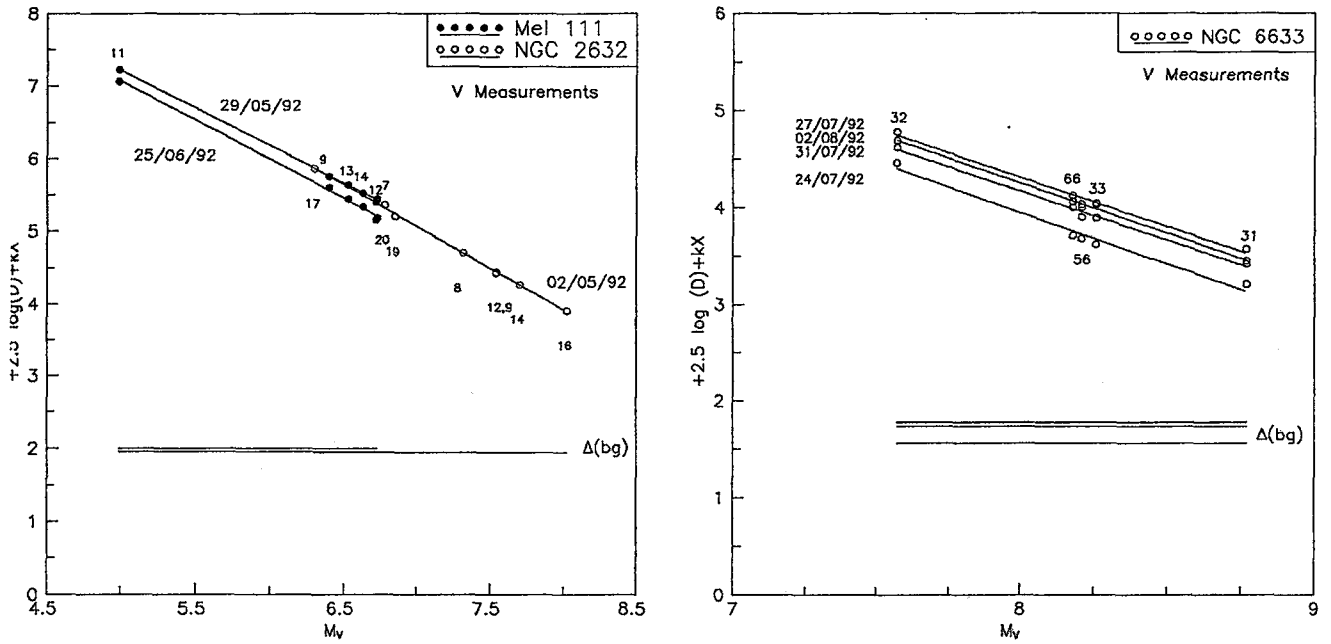

Figure 2.7. Instrumental versus standard V magnitudes for Mel 111 (left side), NGC 2632 and NGC 6633 (right side)

then converted to raw instrumental magnitude using the equation B.11. The extinction coefficients used are obtained from the longest observation of NGC6633 which are k_v=0.4 and k_b=0.5. Then the graphs of assigned V or B magnitudes versus calculated raw magnitudes of v or b are plotted and a linear regression is done for each cycle (for NGC 6633 only a sample cycle is plotted for each night) (figure 2.7 and 2.8). For each cycle, also the background level is drawn. Variation of the background level depends on the total amplifying system and its noise, and the overall average magnitude of the observed cluster stars. For Mel 111 and NGC 2632, magnitude range is between $4^m.99$ and $8^m.21$, and for NGC 6633 all stars have magnitudes greater than $7^m.57$.

To find a compact limiting magnitude, all the data averaged star by star. In NGC 2632, there were only one cycle, so reading error of the deflections are taken as the

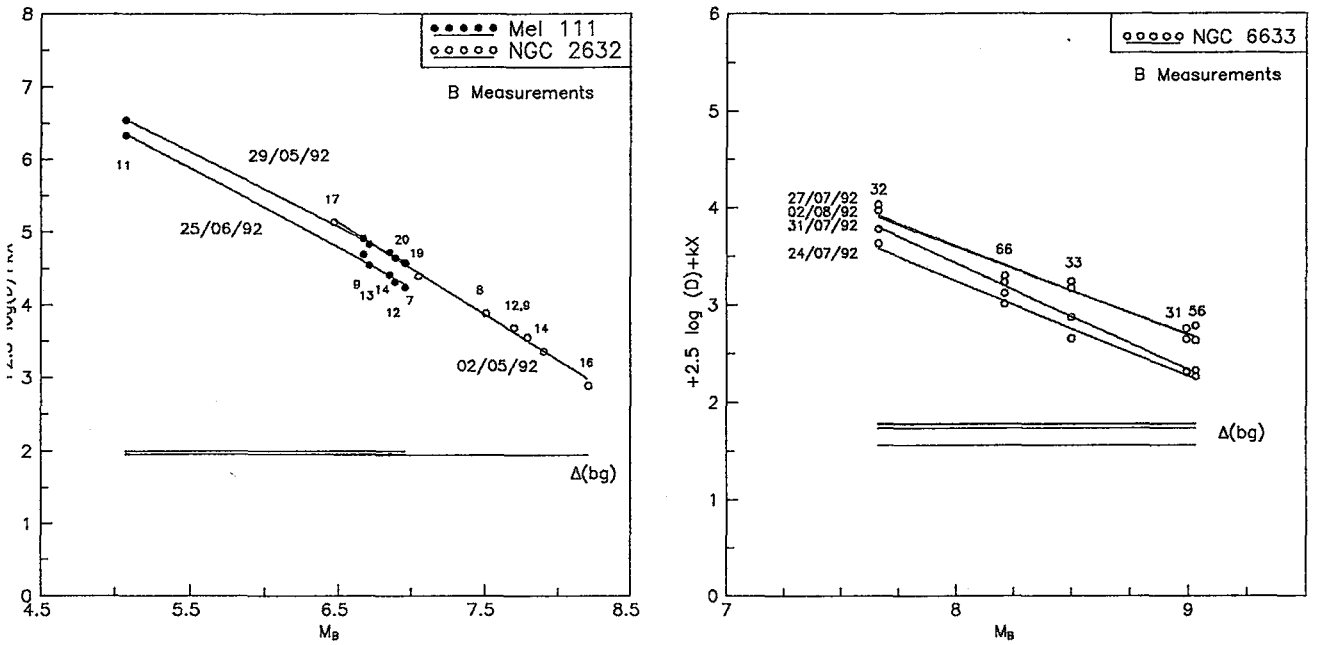

Figure 2.8. Instrumental versus standard B magnitudes for Mel 111 (left side), NGC 2632 and NGC 6633 (right side)

error of the deflection, in Mel 111 there were two cycles, thus average of the deflections are taken and error of the average is evaluated according to root-mean-square deviation of the deflections from the averages. In NGC 6633, however, error of the average is calculated in the following way (example is for V filter):

- Average of the deflections is calculated ($\overline{v}$).
- Standard deviation of the deflections (for one star) gives us the error in the observed deflections (σ_v).
- Upper and lower limits of the averages are calculated by using the equation $\overline{\Delta v_{\pm}} = 2.5\log(deflection \pm \sigma_v) + kX$.
- Thus the errors of the average are calculated by averaging the upper and lower

Table 2.12. Limiting magnitudes obtained from linear regressions of standard versus instrumental magnitudes for both V and B filters

	V	B
a	-1.01	-1.02
b	12.13	11.56
ϵ_y	0.08	0.12
ϵ_x	0.02	0.03
R^2	0.99	0.99
LM_0	10.16	9.50
ϵ	$\pm$0.13	
$\overline{BG}$	1.89	

limits ($v = \overline{v} \pm \overline{\Delta v_{pm}}$).

For background levels, average of all background measurements are calculated and standard deviations of all background levels are taken as the error of the background level for each cluster.

Results show a linear relation between assigned standard magnitude and instrumental magnitude in both filter (figure 2.9). Evaluated values are listed in table 2.12, where a and b are the coefficients of the linear regressions, ϵ_y and ϵ_x are the deviations of the points from the average, R^2 is the corelation coefficient of the regression, LM_0 is the limiting magnitude for *'zero'* deflection, ϵ is the standard deviation of the background level which gives the error of any deflection reading, and $\overline{BG}$ is the average of the background which is the threshold level for any reading. This relation gives us directly the limiting magnitude of the site for V and B filters.

In B filter, points are scattered and the errors are large compared to V filter. This is mainly due to the photometer itself. Since SSP-3 uses a silicon diode for measurements, its response for blue region of the spectrum is low compared to red region. However the effect of this inability is not much in the calculations of the limiting

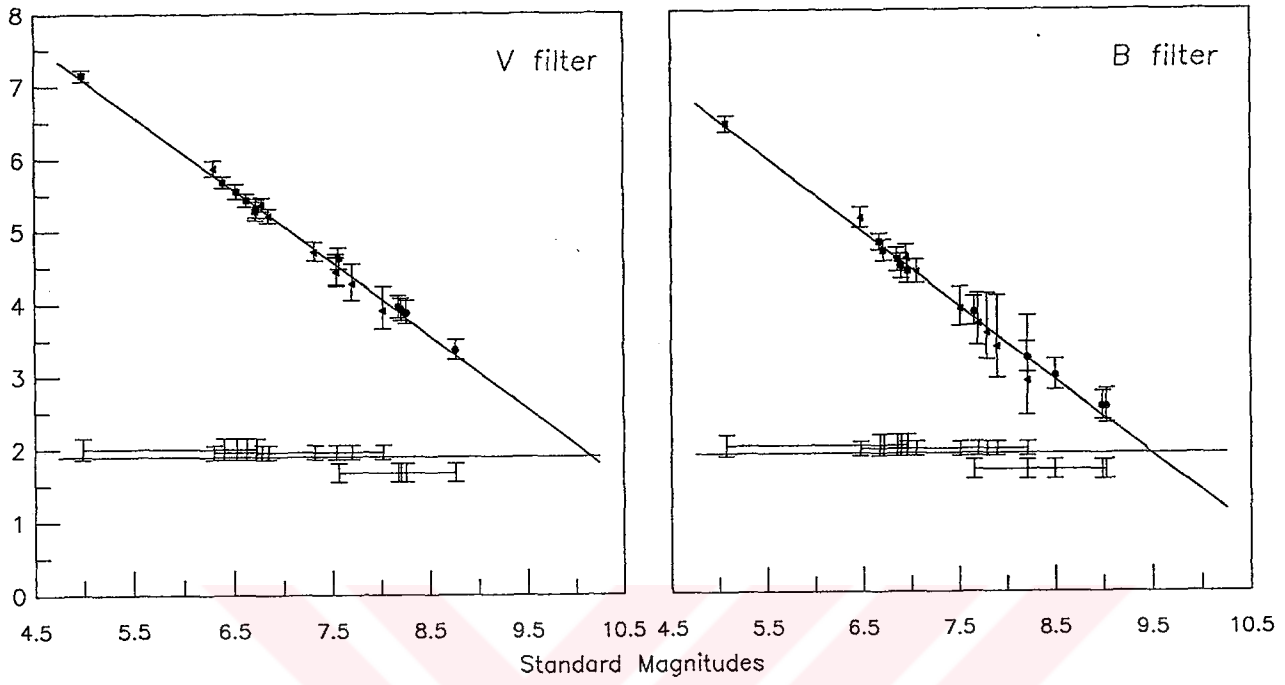

Figure 2.9. Instrumental versus standard magnitudes for V (left) and B (right) filters

magnitude for B filter.

Note that all the observations of NGC 6633 were in zenith direction, however other clusters have airmasses between 1.1 and 1.4. Combined and reducted values gives a linear relation with an error of 0.08 (0.12) in instrumental raw magnitudes for V (B) filter and error of the linear regression calculations is 99%. Therefore it can be said that the effect of airmass is eliminated successfully. For ideal case slopes should be exactly one. Deviation from this value can be eliminated by using transformation coefficients.

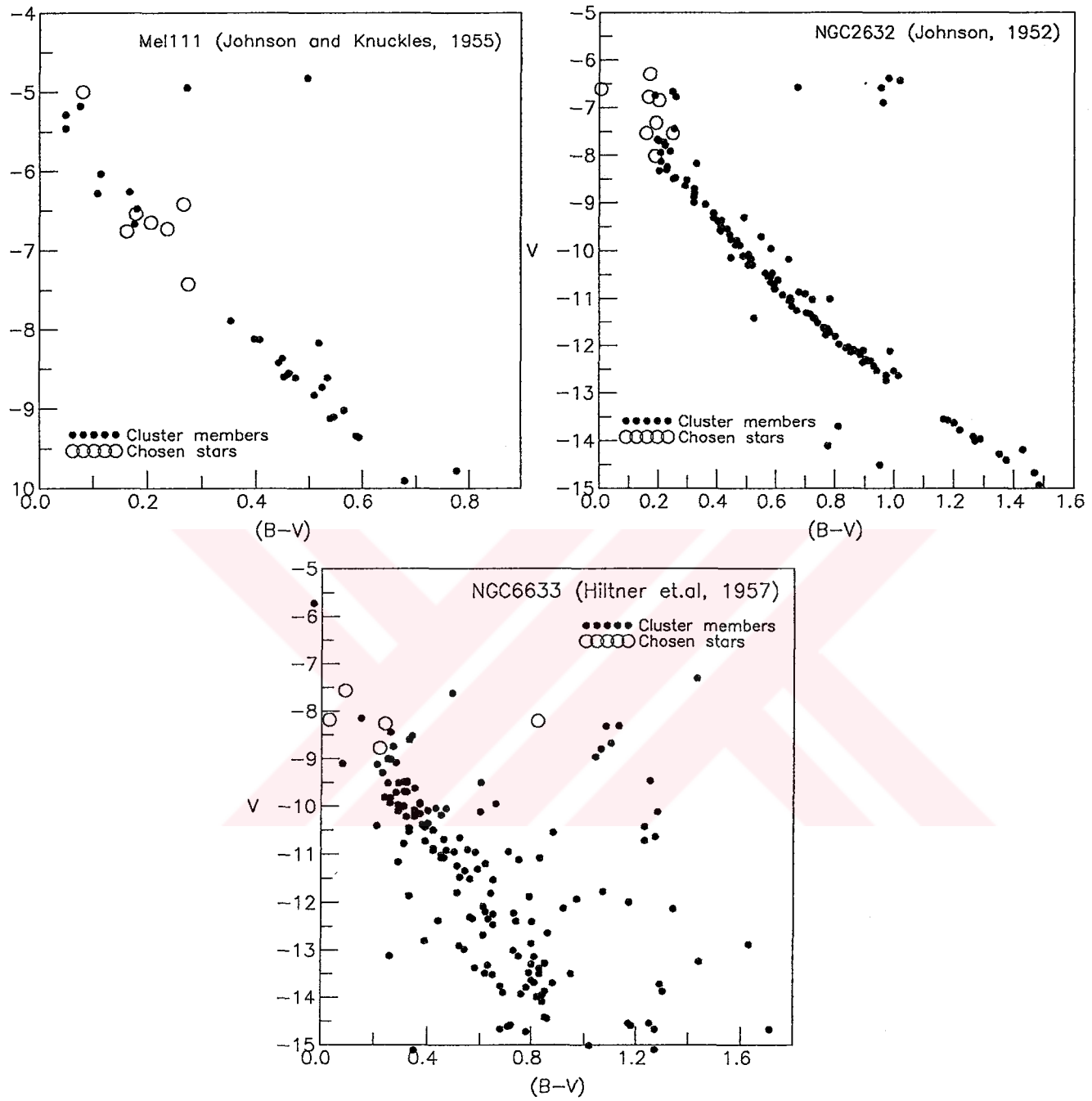

Figure 2.10. V versus (B-V) graphs of the clusters NGC 2632 (top left), Mel 111 (top right), NGC 6633 (bottom)

CHAPTER III

CALIBRATION OF THE CCD CAMERA AND OBSERVATIONS

3.1 History of CCD

The charge-coupling principle was invented by Boyle and Smith (1969). First demostration of such a device is done by Amelio, Tomsett, and Smith at the Bell Laboratories, in USA with one-line and eight-pixel format. Larger formats (i.e 100x100 pixels), however, were not introduced until 1973. The first devices were called *surface-channel* CCD's, because when light is absorbed, formed electrical charges will be stored and treated near the surface of the silicon. Difficulties with this kind of structure led to a more complex architecture, called *buried-channel.* After the idea and construction of such devices, noise techniques had to be developed to make better transistor amplifiers on the CCD itself, to invent electronic filtering circuits to 'condition' the CCD signals, to improve the quality and the stability of power supplies, and to find ways of manufacturing CCDs reliably in large quantities free of microscopic defects which could affect hundreds of otherwise good pixels.

The basic principles of semiconductors and CCD chips, and fundamental observing and correcting sequences of the image frames are discussed in appendix **??**.

3.2 Observations

3.2.1 Calibration Observations

The flat-field calibration method is used in this work (SSU User Package, 1990 and Tyson 1986). The light source stability and white illumination is obtained in a dark room. The CCD and light source are aligned on a optical bench.

Table 3.1. Measurements of flat-field histograms of the observed images

t	n_{med}	σ
10	58	6.5
20	107	7.5
30	162	7.5
40	215	8.0

Gain is arranged so that the bias level of the lowest exposure time is within 20-30 ADU (Gain=0 Offset=128). With this reference level, 10, 20, 30, and 40 seconds of exposure times are chosen. Also with these exposures, the linear relation between exposure time and signal level is satisfied. No over or under exposure occurred, which satisfies the bias level. The resultant measurements of the histogram of the flat-field images are shown in table 3.1, where t is the exposure time, n_{med} is the median signal level of the image histogram, and σ is the standard deviation of the image histogram at FWHM.

Table 3.2. Results of the linear regressions (n_{med} vs. t and variance vs. bias corrected n_{med}) (top) and calculated system parameters from the linear regressions (bottom)

n_{med} vs t	→slope	5.26	ADU/sec
	→y-intercept	4.00	ADU
σ^2(n) vs n_{med}	→slope	0.062	ADU/electrons
	→y-intercept	19.23	ADU^2

system gain	g	0.062	ADU/electron
	$p = 1/g$	16.13	electron/ADU
readout noise	R	4.39	ADU
	$r = R/g$	70.73	electrons

Using these values, the median values versus exposure time (figure 3.1) and variance versus bias corrected signal level (figure 3.2) graphs are plotted. Since, each exposure is repeated twice, variance (σ^2) should be divided by two. Results of the

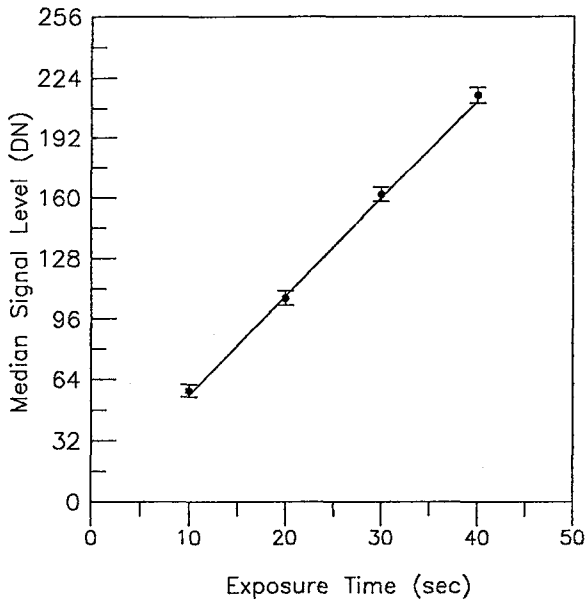

Figure 3.1. n_{med} versus t graph for the flat-field observations

linear regressions applied to both graph are shown in table 3.2 (top panel). From the regression parameters, calculated system settings are also shown in table 3.2 (bottom panel).

Thus to correct an image for flat-field with these settings, one can use a reference frame used in the flat-field exposures which must belong to the middle of the linear part of n_{med} vs. t graph. With this frame, flat-fielding is done in the following manner:

$$p^c_{(i,j)} = \frac{p_{(i,j)}}{f_{(i,j)}} \times \frac{\sum_{k=1}^{100} f_{(*,*)}}{100} \tag{3.1}$$

where $p^c_{(i,j)}$ is the flat-field corrected pixel value, $p_{(i,j)}$ is the original pixel value, $f_{(i,j)}$ is the corresponding pixel value for the flat-field frame, $f_{(*,*)}$ is the randomly chosen pixels from the flat-field frame. This procedure normalizes any frame with the knowledge of the response of the CCD pixels.

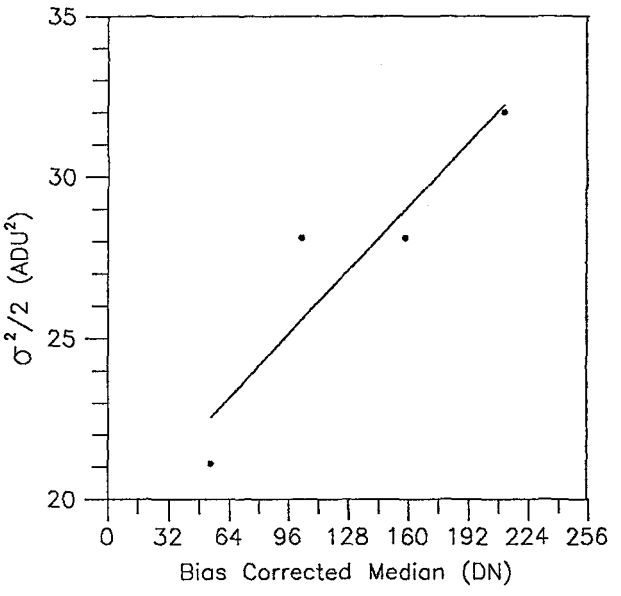

Figure 3.2. Variance versus Bias corrected n_{med} graph for the flat field observations

3.2.2 Observations with Standard Stars

NGC 6633 is also used in the CCD observations. The same stars are chosen also. Since the image frame size of the CCD covers 6'×5' field of view, stars #31 and #32 were in one frame and #56 and #66 were in another frame. The median sky values was in the same order for both frames, so dividing the field into two made no effective error in final analysis of the magnitudes.

Exposure times and gain/offset settings were constant during the observation: gain setting was 0, offset setting was 128 which are the same values obtained from flat-field calibrations. Exposure time was set to 1.3 seconds which prevents over exposure of the star #32; the brightest among the group. The temperature of the CCD was greater than -80°C and before the cooling process, CCD camera vacuum maintenance was carried out. Again, observation is done on a clear night (August 8, 1992). Totally eight observations were done, which made 16 frames in approximately 23 minutes.

Since dark frame were missing for the observation, only flat-field correction is performed for each frame. After the reduction of the frames, the magnitudes are determined with the SSU software package. The software estimates the magnitudes in the following way:

- The sky value around the star is determined by choosing an annulus with user fed inner and outer radius values at a center of an ellipse (calculated from the cursor position on the frame).
- Then by using calculated (or assigned by the user) *threshold above the sky* value, the star histogram around the centroid is obtained.
- Finally, at a point approximately 1.5×FWHM of the centroid point it calculates the pixel value, which gives directly the brightness of the star for calculated sky value. Thus the magnitude of the star is calculated by using the equation D.2 with a constant ZP value (can be changed for a site or on optical arrangement), and without air-mass or color correction.

By using the above procedure the magnitudes (since there are no installed filters in the CCD configuration, calculated magnitudes represent the clear filter response of the CCD) are calculated and listed in table 3.3, where # is the star number, first character of the frame number is the observation number and the second one is the frame number (a: stars of #31 and #32, b: stars of #66 and #56), sky is the median sky value of the frame, th is the threshold above the sky value for that star, S/N is the signal-to-noise ratio of the star at centroid point which is obtained from the magnitude calculation routine of the SSU package, and m is the clear (whole spectrum) magnitude of the star.

Table 3.3. Observations of NGC6633 with CCD (contains two frames)

#	Frame	Time	Sky	th	S/N	m
31	1a	20:21:32	21.6	34	30.0	11.54±0.04
	2a	20:31:25	24.4	38	42.7	11.30±0.03
	3a	20:33:31	25.3	38	33.7	11.23±0.03
	4a	20:35:32	22.8	35	38.2	11.43±0.03
	5a	20:38:25	25.4	35	26.7	11.49±0.04
	6a	20:40:20	22.6	32	27.0	11.52±0.04
	7a	20:41:57	24.5	35	30.5	11.41±0.04
	8a	20:43:57	26.4	39	38.4	11.36±0.03
32	1a	20:21:32	21.6	34	178.8	9.62±0.01
	2a	20:31:25	24.4	38	169.0	9.61±0.01
	3a	20:33:31	25.3	38	165.4	9.57±0.01
	4a	20:35:32	22.8	35	168.4	9.66±0.01
	5a	20:38:25	25.4	35	154.6	9.62±0.01
	6a	20:40:20	22.6	32	153.4	9.70±0.01
	7a	20:41:57	24.5	35	171.5	9.65±0.01
	8a	20:43:57	26.4	39	170.3	9.66±0.01
66	1b	20:29:23	26.9	40	84.4	10.46±0.01
	2b	20:32:44	22.6	35	93.9	10.48±0.01
	3b	20:34:31	25.4	35	81.7	10.52±0.01
	4b	20:37:43	23.4	32	79.1	10.69±0.01
	5b	20:39:34	25.6	34	89.5	10.64±0.01
	6b	20:41:19	24.5	33	77.6	10.68±0.01
	7b	20:42:45	23.5	36	89.5	10.51±0.01
	8b	20:45: 6	23.5	35	88.9	10.69±0.01
56	1b	20:29:23	26.9	40	135.2	10.01±0.01
	2b	20:32:44	22.6	35	136.5	9.88±0.01
	3b	20:34:31	25.4	35	124.2	10.12±0.01
	4b	20:37:43	23.4	32	139.3	10.03±0.01
	5b	20:39:34	25.6	34	142.1	9.95±0.01
	6b	20:41:19	24.5	33	107.9	9.97±0.01
	7b	20:42:45	23.5	36	149.9	9.90±0.01
	8b	20:45: 6	23.5	35	149.2	10.03±0.01

With these magnitude information, relation to the standard magnitudes for CCD can't be done. However system response and frame settings can be arranged by the analysis of these frames. To obtain such information, magnitudes of three stars (#45, #42, and #41), appearing in *a* frames are also calculated and listed in table 3.4. Here S/N is a measure of the star's brightness against the sky value at that centroid point.

These three fainter stars have small S/N compared to stars #31 and #32 on the same frame. Plotting S/N versus magnitude, shows that to have an accurate

Table 3.4. Observations of the stars #45, #42, and #41 (stars are on the first frame)

#	Frame	Time	Sky	th	S/N	m
45	1a	20:21:32	24.9	36	33.4	11.83±0.03
	2a	20:31:25	24.9	39	33.7	11.71±0.03
	3a	20:33:31	21.6	32	33.0	11.83±0.03
	4a	20:35:32	25.7	34	30.7	11.80±0.04
	5a	20:38:25	23.7	32	30.0	11.82±0.04
	6a	20:40:20	23.7	31	27.5	12.03±0.04
	7a	20:41:57	23.4	32	29.2	11.86±0.04
	8a	20:43:57	24.3	36	26.9	12.04±0.04
42	1a	20:21:32	24.8	36	10.5	12.93±0.10
	2a	20:31:25	27.7	39	16.8	12.48±0.06
	3a	20:33:31	20.8	32	23.6	12.17±0.05
	4a	20:35:32	23.8	34	11.5	12.82±0.10
	5a	20:38:25	23.3	32	16.7	12.57±0.07
	6a	20:40:20	23.6	31	16.5	12.62±0.07
	7a	20:41:57	23.2	32	10.3	12.99±0.11
	8a	20:43:57	28.7	36	20.1	12.23±0.05
41	2a	20:31:25	29.8	39	9.6	13.07±0.11
	3a	20:33:31	21.9	32	13.4	12.87±0.08
	4a	20:35:32	25.9	34	11.8	12.83±0.09
	5a	20:38:25	23.6	32	9.1	13.14±0.12
	6a	20:40:20	23.5	31	16.6	12.59±0.07
	7a	20:41:57	21.9	32	23.0	12.24±0.05
	8a	20:43:57	24.7	36	18.2	12.52±0.06

estimate of a magnitude, star value (S/N) should be higher enough than the threshold value or considerably away from the sky background (sky). Practically this limit can easily be obtained from the figure 3.5. For stars #31, #32, #66 and #56 magnitude variations are small compared to stars #42 and #51 where as the S/N increases magnitude gets brighter. However, as a limiting case, at the S/N value of around 30, the magnitude variations are stabilized for the stars #31 and #45. This gives us a limiting value for the signal-to-noise ratio.

Having a lower limit for the S/N value is not enough for a frame analysis. If an over exposed image is considered the pixels will be full (no number can be generated for this value by the computer) so that no magnitude estimation can be carried out due to lack of information about the moment when it is over exposed first. Thus the upper limit for the system settings can be found by setting the exposure time.

Limit can be achieved by observing the same frame for different exposure times with the same settings of the CCD. This work is done for the stars of the first frame, on the night of June 24, 1992. Unfortunately, the gain setting of the CCD was 128 instead of 0. Since, our frame size is big enough (512×480), the flat-field correction will not differ so much if the reference flat-field frame has a gain setting of 0.

Again flat-field corrections are carried out and estimated magnitudes and S/N values are obtained by using the SSU software package. Then for each star, graph of S/N ratio versus exposure times is drawn in figure 3.6. The star number #217 is due to Sanders (1972). V magnitudes are shown at the top of lines. Points that are represented by 'x', are the stars that appeared only on the frame of 60sec

The last values for each star, represents exposure times before the over exposure. As expected, the brighter stars saturates at lower exposure times or vice versa. If the star's S/N is calculated at a exposure time which is close to the over exposure time, we observe very high S/N for the overexposed times (e.g stars #45 and #51). Since the relation between exposure times and S/N ratio is linear, taking half of the overexpose times gives the proper exposing time for the object.

3.2.3 Sample Observations of Comet Swift-Tuttle

In the IAU telegram 5330, the discovery of the Comet Swift-Tuttle was reported, which is observed first by Kegler in 1737 (II). The discovery is confirmed by other observations, by seperating its location from the Perseid meteor shower (IAU Telegrams 5586, 5620).

At the end of October 1992, its magnitude was estimated by the observers to be around 7-8. Since weather conditions prevented a long period observation of the comet, in this work, observation was only possible in October 21, 1992. Four frames of

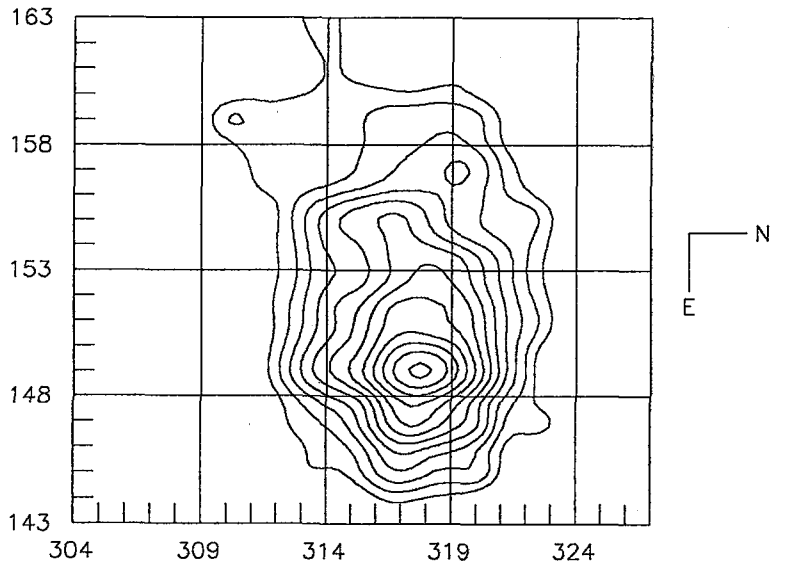

Figure 3.3. Topographical plot of the comet. It is taken from 75^s exposure time. Axes represent the frame pixels. Approximately North is to the right, East is to the bottom.

the comet were taken. The time between first and last frames was 15 minutes. In that interval, change of its position is observed (figure 3.7). By widening the annulus size of the magnitude calculation routine, the clear magnitude of the comet is estimated *roughly* as $7^m.1$-$7^m.4$.

In the frame of 75^s, the tail of the comet is considerably visible. To find the tail direction, topographical plot of the comet region is plotted in figure 3.3. Coma direction is roughly estimated to be in East, and size of the coma is approximately $6''.4$, which are confirmed by the IAU telegrams.

To find a rough value for the apparent velocity, object positions are shifted according to star coordinates of the first frame. Final combined positions of the three stars and the comet for four frames are shown in figure 3.4. By calculating six possible different intervals, the apparent velocity of the comet is found to be 5.23 pixel/min

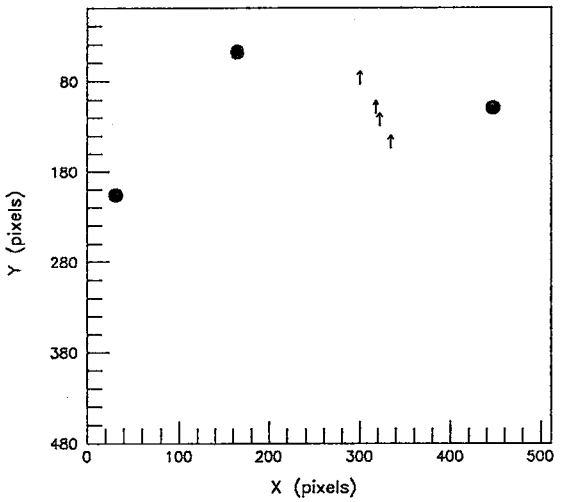

Figure 3.4. Movement of the comet. The positions are shifted according to the objects positions of the first frame by fixing the first frame positions.

which gives 4.19 arcsec/min. Since in that time, there were no apparent velocity calculation of the comet, by interpolating the daily variation of the comet position (where these positions were calculated from the early estimation of the orbit parameters) the apparent velocity of the comet is found to be 5.88 arcsec/min.

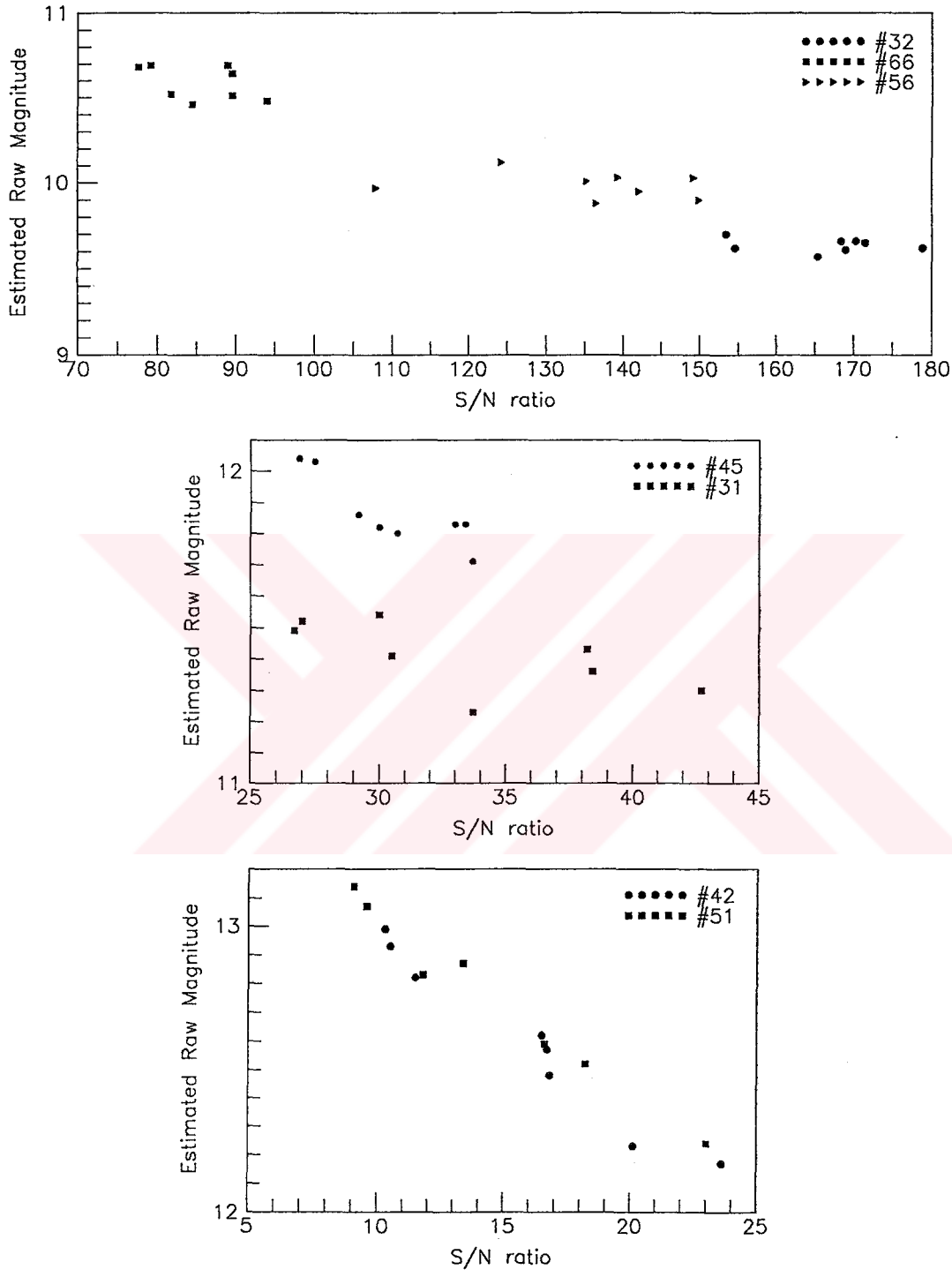

Figure 3.5. S/N versus estimated raw magnitudes (with no filter) for the cluster stars

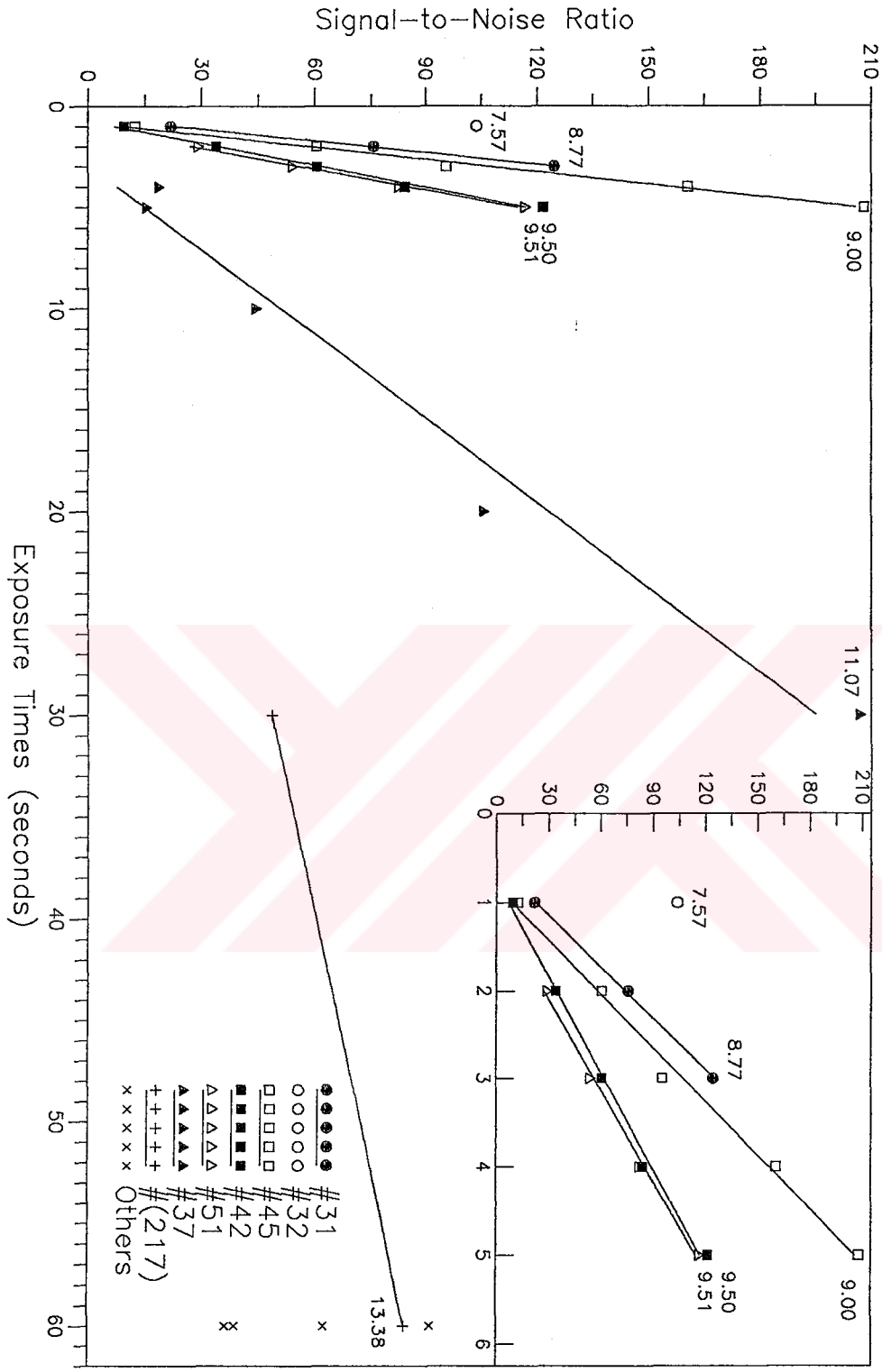

Figure 3.6. Exposure times vs. S/N ratio of the star #31, #32, #66, #56, #45, #42, #51, #37, and #(217)

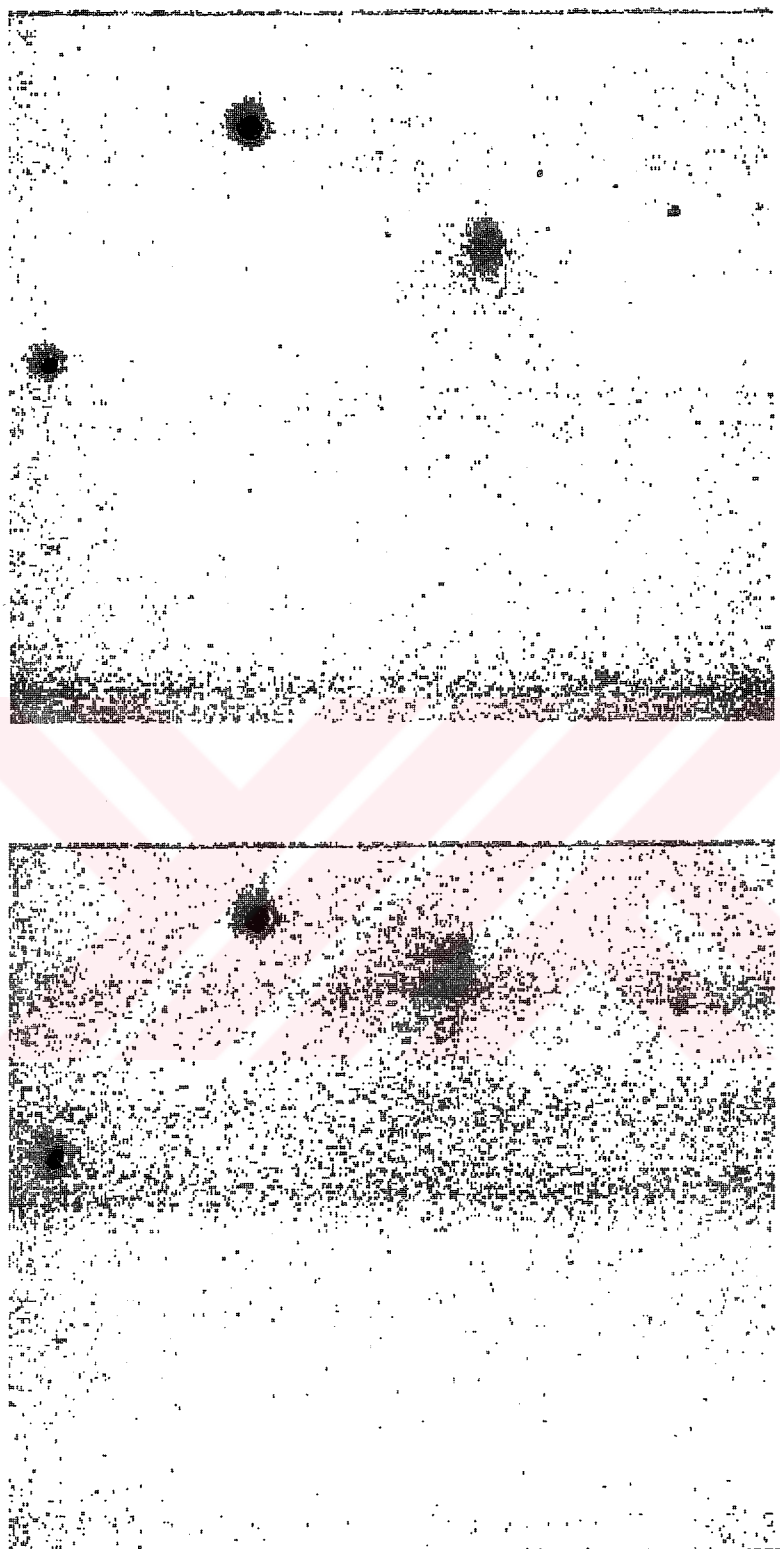

Figure 3.7. Comet Swift-Tuttle. At the time 19:15 UT (top) and 19:23 UT (bottom) for the October 21, 1992

CHAPTER IV

CONCLUSION

As explained in chapter 2 and 3, the main parameters of the site are measured or calculated by using proper methods and instruments. Since basic aim of the work was to find the limits of the site with the installed instruments, explanation of the instruments are also given in appendix A.

The first point to look for was the geographic position of the observatory. To have the longitude and latitude correctly, theodolite is used in the observations (Nikon NT-4D). Maintaining the leveling error constant, results of the calculations gave accurate values (detail explanations of the method is discussed in chapter 2):

$$\lambda = 32^{o}46'28''.2 \pm 1'09''.5$$

$$\phi = 39^{o}54'10''.2 \pm 1'04''.1$$

Since, the main pollution comes from the city light, its position and approximate value should be known for any future observation program. With a proper instrumentation, which is discussed in chapter 2, the locations of the main source of light pollution, accumulated with the air pollution, is found. The clear windows in the sky deviates from zenith to the south direction. However, this was in the year 1992. Now there are excavations (new buildings of Bilkent and YÖK), which are taking place at the azimuth of that direction. Thus every year the survey of the background light should be done for safety. Since it takes only 40 minutes to record everything and if the survey is done monthly, a log-book of the open windows of the sky can be obtained accurately.

There are two main installed observing instruments in the observatory.

One of them is the SSP-3 photometer. Using this photometer and V and B filters of Johnson filter set, the limiting magnitude of the site according to the physical limit of the instrument, is found to be

V	10.16±0.13
B	9.50±0.13

In practice, however, this values very high. As the site gets worse every year, observations with SSP-3 gets more difficult and more unreliable, if observations are not done repetitively or for a long time.

The second installed instrument is the CCD camera. Since the instrument itself is new to everyone, every work concerning the camera is done for the first time. And it should be said at first that all the observations, including the calibration observations, must be repeated with proper filter sets, which will be used in future works, and with all the gain/offset settings of the camera.

Common calibration methods are used in this work. Each frame is corrected for flat-field and then used for analysis. Main aim of the work for this instrument was to find basic limits of the observations and the instrument. Since no filter is used in the observations, all calculated magnitudes corresponds to *clear filter*. Observations are done for the highest gain setting.

A reliable lower limit for S/N ratio and an upper limit for the exposure times are found. Since camera works by accumulating the electrons falling on each pixel, over and under exposure of the objects must be prevented by analyzing histogram of the corrected frame.

If the CCD camera is compared with SSP-3, the limit of the SSP-3 is achieved by a 5 second exposure time. This much of exposure saturates a 9.50 V magnitude star. A realiable magnitude calculation can be processed successfully, if the

object has a S/N greater than 30 ADU, which can be interpreted as the lower limit of the instrumentation. Upper limit can be arranged by adjusting the exposure times. Thus for a 9.00 V magnitude star, with an exposure time of 3-4 seconds, it will have a S/N ratio of 120, which is considerably higher than the threshold above sky and the lower limit of the camera, and lower enough than the over exposure time (5 seconds). However this limits will change when filters are used. Since clear filter magnitudes are higher than the V magnitudes. we would expect a decrease in the limits.

Software used in the magnitude calculations and other camera and computer controls are enough for the time being. However, if accurate observations are needed and much manipulations in the calculations are required then a new software must be written or used. MIDAS, ROMAFOT, DAOPHOT or SURFPHOT like software packages are best for photometry. In future works adaptation of the CCD image to MIDAS will be done.

REFERENCES

Allen, C.W., 1973. Astrophysical Quantities, Athlone Press, London.

Aoki, S., Guinot, B., Kaplan, G.H., Kinoshita, H., McCarthy, D.D., and Seidelmann, P.K., 1982. Astron. Astrophys., 105, 359.

Aslan, Z., Aydın, C., Tunca, Z., Demircan, O., Derman, E., Gölbaşı, O., and Marşoğlu, A., 1989. Astron. Astrophys., 208, 385.

Becker, W., Fenkart, R., 1971. Astr. Astrophys. Suppl., 4, 241.

Blitzstein, W., Fliegel, H.F., Kondo, Y., 1970. Applied Opt., 9, 2539.

Bomford, G., 1971. Geodesy, Clarendon Press, Oxford.

Boyle, W.S., and Smith, G.E., 1971. IEEE Spectrum, 8, 18.

Hagen, J.B. and Boksenberg, A., 1991. The Astronomical Almanac, U.S. Government Printing Office, Washington.

Hagen, J.B. and Boksenberg, A., 1992. The Astronomical Almanac, U.S. Government Printing Office, Washington.

Hall, D.S., Genet, R.M., 1982. Photoelectric Photometry of Variable Stars, Minuteman Press.

Hall, R.T., and Rawcliffe, R.D., 1971. Applied Opt., 11, 468.

Hardie, R.H., 1962. Astronomical Techniques Ch. 8, p178.

Johnson, H.L., 1952. Astorphys. J., 116, 640.

Johnson, H.L., 1955. Ann.Astrop., 18, 292.

Johnson, H.L., 1963. Basic Astronomical Data, p.204, University of Chicago Press, Chicago.

Johnson, H.L., and Harris, D.L., 1954. Ap.J., 120, 196.

Johnson, H.L., and Knuckles, C.F., 1955. Astrophys. J., 122, 209.

Johnson, H.L., Mitchell, R.I., Iriarte, B., and Wisniewski, W.Z., 1966. Comm. of Lunar and Planet. Lab., 4, 99.

Johnson, H.L., and Morgan, W.W., 1953. Ap.J., 117, 313.

Landolt, A.U., 1973. A.J., 78, 959.

Landolt, A.U., 1983. Astron. J., 88, 439.

Mackay, C.D., 1986. Annual Rev. of Astron. & Astrophys., 24, 255.

McInnes, B., 1981. Q.J.R. Astr.Soc., 22, 266.

McLean, J.S., 1989. Electronic and Computer-Aided Astronomy, Camelot Press, Southampton.

Montenbruck, O., 1989. Practical Ephemerides Calculations, Springer-Verlag Press, Berlin.

Nikon NT-4D Instructions Manual, Tokyo.

Optec Inc., 1984. SSP-3 Manual.

Plass, G.N., and Kattawar, G.W., 1971. Applied Opt., 10, 2304.

Sanders, W.L., 1972. Astron. Astrophys. Suppl., 9, 213.

Sonoma State University, 1990. SSU User Package.

Stobie, R.S., Gilmore, G., Reid, N., 1985. Astron. Astrophys. Suppl., 60, 495.

Tyson, J.A., 1986. J. Opt. Soc. Am. A., 3, 2131.

White, M.H., Lampe, D.R., Blaha, F.C., and Mack, I.A., 1974. IEEE J. Solid-State Circuits, 9, 1.

Yaşar, K. 1991. (Special Communications).

Young, A.T., 1971. S & T 139.

APPENDICES

APPENDIX A

INSTRUMENTATION OF THE OBSERVATORY

A.1 Observatory

Name	METU Observatory
Construction Year	1986-1989
Start of Observations	1991
Electricity	220 Volt, three phase, 6.5kW
Living Section	Bedroom, bathroom, kitchen
Laboratory Section	Machinery and control room
Dome Diameter	5 meters
Dome Control	Fast motion with motors, slew motion is manual
Observing Slice of Dome	90°
Observing Slice Control	With motor
Pillar Dimensions	0.8x0.8x7 meters
Computer	IBM AT compatible 386 computer, 40M hard disk

A.2 Telescope

Company	Group 128 Inc.
Model No.	117
Manufacturing Year	1975
Aperture	16 in., 40cm
Focal Ratio	f/11
Optical System	Cassegrain
Optical Material	Pyrex
Coating	Aluminum
Primary mirror cell	9-point flotation with tilt adjustment
Secondary mirror cell	Cup with independent tilt and translation
Focusing method	With stepper motors
Mounting type	Asymmetric equatorial with extended polar axle
RA Track Rate	10-20 arcsec/sec
RA Guide Rate	2-15 arcsec/sec
RA Set Rate	30-90 arcsec/sec
Dec Guide Rate	2-15 arcsec/sec
Dec Set Rate	30-90 arcsec/sec
Drive Gears	360-tooth worm wheels and ground worms
Overall weight	450 kg.
Overall height	2.5 meters

A.3 SSP-3 Photometer

Name	OPTEC SSP-3 (Solid State Photometer)
Detector Type	Silicon PIN-photodiode
Detector Diameter	1mm
Spectral Range	300-1100 nm
Electrometer	Current-to-Voltage
Gain of the Electrometer	5×10^{10}
Maximum Output Voltage	4.0 Volt
A/D Converter	Voltage-to-Frequency
Full Scale	10 kHz
Full Scale Input Voltage	-6.6V/-660mV/-66mV
Integration Time	1 and 10 seconds
Timer	R-C Circuit
Power Supply	9 Volt NiCd
Operating Time	5 hours
Recharge Time	15 hours
Battery Charger	12 Volts DC, 100mA
Eyepiece Focal Length	25 mm
Field of View	0.4^{o}
Filters Type	Schott Colored Glass
Filter Set	Johnson

A.4 Astro-Link CCD Camera

Name	Astro-Link, Cryocam 80
Chip Size	8.8mm×6.6mm
Pixel Size	512×480
One Pixel Unit	0.8 arcsec
Cooling	Peltier cooler
Thermal Insulation	Thermos bottle vacuum technique
Detector Temperature	-80°C
Cool Down Time	35 minutes
Electron Noise	< 20 electrons
Windows	Coated BK7 glass

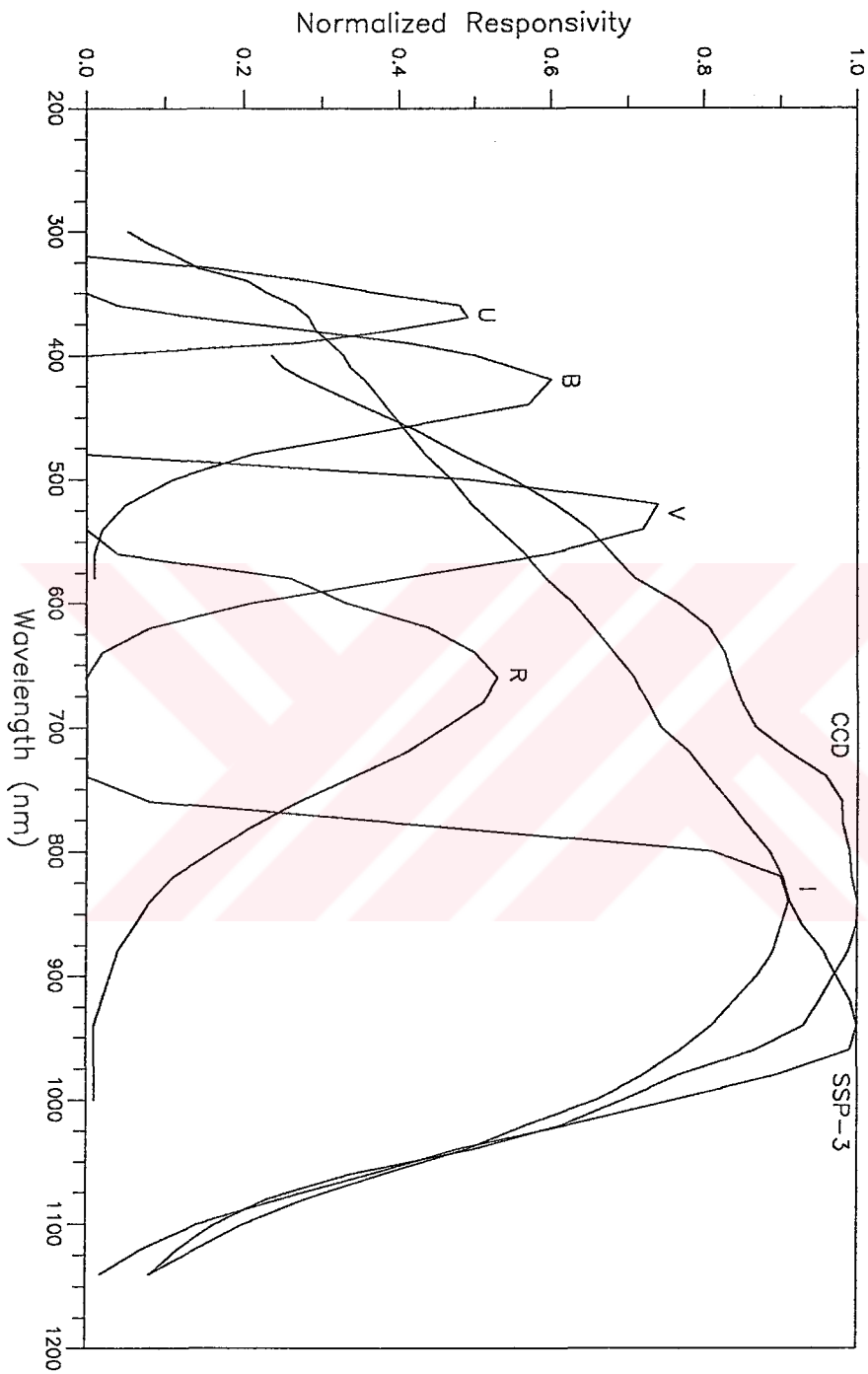

Figure A.1. Spectral Responses of SSP-3, its filters and Astro-Link Camera

APPENDIX B

OBSERVATIONAL ASTRONOMY AND ITS BASIC DEFINITIONS

An observation is normally meaningful only as part of a pattern, a model of the situation into which the observation can be fitted and through which it can be interpreted. If we consider ordinary light, the only things we can hope to observe directly will be

1. position on the sky from which the light appears to come and change of this position with time,
2. brightness of the light at particular frequencies (colors) or over certain ranges of frequencies and change of such brightness with time,
3. polarization of the electric and magnetic fields in the radiation

Thus classical astronomy dealt only with the direction to the light source and made only very slight use of the information carried by light and variation of it. Observations of brightness, in particular at each wavelength with the light spread out into a spectrum, are necessary to make the picture more complete. Study of the brightness and its variations is the main tool of an astronomer. And as a tool, photometry is used for the measurement of the *total* brightness of stars and other objects. In astronomy, photometry is used mainly for

- comparison of the brightness of different stars in the same broad spectral band,
- measurement of different broad-band spectral regions in the light of a particular star, and
- following of variations of brightness of a single star.

Of course it is not really possible to measure the total light from ground based sites since atmosphere, instrument and light-detector impose limits on the spectral region.

B.1 Magnitude Scale

First classification of the stars is carried out by Hipparchus, according to their brightness. He graded the stars into six groups. This classification was a linear, natural intensity scale.

Magnitude scale has reached its modern basis by Pogson (1856). He defined a system such that each magnitude interval corresponds to a factor of exactly $\sqrt[5]{100} = 2.512$ in intensity and analytically this means that the ratio of intensity of two stars must correspond to their difference of magnitude;

$$\begin{aligned} \frac{I_1}{I_2} &= \left(\sqrt[5]{100}\right)^{(m_1-m_2)} \\ \log\frac{I_1}{I_2} &= \log(10)^{\frac{2}{5}(m_1-m_2)} \end{aligned}$$

Thus

$$m_1 - m_2 = -2.5\log\frac{I_1}{I_2} \tag{B.1}$$

B.2 Color System

A color system is required for the observation of brightness. You have to have the information coming from the light in all of the spectrum. But this is not an easy process to achieve. Rather, you can restrict your window into some smaller bands by using a coated glass with some special solutions (filter). Since, this glass will have a transmittance curve for the incident light where it has a different response for different wavelengths. So the light that you wanted to observe in a specified window throughout the spectrum, can be detected easily.

Difficulty arises when different filters used by different observers. It is overcome by introducing color systems. Spectrum is covered by choosing successive filters where their transmittance curves and coatings are known by every observer.

A standard photometric system is defined by a list of stars each having a magnitude (for each filter) assigned to it. Even the observations of the stars is done in an observatory with a specific instrumentation, the standard system is not defined with the equipment. Rather it is the published magnitudes (standard magnitudes), assigned to certain stars (standard stars). But the magnitudes determined by an observer with different instrumentation are called instrumental magnitude. With this instrumentation, he/she determines, his/her own instrumental magnitude using the standard stars given for that standard photometric system. Then the instrumental magnitudes must be related with the standard values, which is called a transformation. This is a relation which reproduces the standard magnitudes using instrumental magnitudes. Widely used standard photometric systems are as follows:

- UBV system by Johnson and Morgan (1953), and additional refinements were done by Johnson and Harris (1954), Johnson (1955, 1963), and Landolt (1973).
- RI extension to UBV system by Johnson et.al (1966) and further observations of UBVRI were done by Landolt (1983).
- Another RI extension by Kron et.al (1953), and modified by Cousins (1976).
- RIJKLMN by Johnson and Mithchell (1962), and additional refinements were done by Johnson (1965), and Greenstein (1970).
- uvbyβ system by Strömgen (1966).

To be able to have a successful transformation, the photometric system should as closely

as duplicate each spectral response in the standard system, both in effective wavelength and width of the spectral response. In table B.1 effective wavelengths and effective band widths of some standard photometric systems are given.

Table B.1. Effective wavelengths and band widths of standard photometric systems

Filter	λ_{eff} (Å)	$\Delta\lambda_{eff}$ (Å)	Filter	λ_{eff} (Å)	$\Delta\lambda_{eff}$ (Å)	Filter	λ_{eff} (Å)	$\Delta\lambda_{eff}$ (Å)
U	3650	680	R	7000	2200	u	3500	340
B	4400	980	I	9000	2400	v	4110	200
V	5500	890	J	12550	3800	b	4670	160
			K	22000	4800	y	5470	240
			L	34000	7000			
			M	50000	—			
			N	102000	—			

Taking the UBV as an example, the form of a transformation is done in the following manner;

$$V = v_o + \psi_v\,(B-V) + z_v \tag{B.2}$$

$$B = b_o + \psi_b\,(B-V) + z_b \tag{B.3}$$

$$U = u_o + \psi_u\,(U-B) + z_u \tag{B.4}$$

where ψ's are the transformation coefficients and z's are the zero points of the transformations. If you have matched your system precisely with the standard system except the zero points then you would have the ψ values zero. If you have deflection of more then 0.1 from the standard values, then you might have a non-linear transformation. If ψ_v is positive (negative), then v response lies to the red (blue) of the response.

Zero points are affected by so many parameters originating especially from the telescope and the detector. To have a stable photometry the zero points should be

maintained constant throughout observation night. For differential photometry however, it is required that the zero points should remain constant for shorter intervals during a night. Some factors for determining the zero points are as follows;

- photomultiplier's sensitivity,
- filter halfwidths and peak transmissions,
- amplification factor,
- integration time of the detector,
- sensitivity of the chart recorder or recording device,
- scale of the deflection on the chart paper.

And the affects which will change the zero points are as follows;

- cleaning or realuminizing the mirror of the telescope,
- dirty filter glasses or optical elements,
- changing amplifier(s) or voltage supply of photomultiplier(s),
- changing gain settings on the chart recorder,
- changing the orientation of the photomultiplier tube,
- exposing the photocathode to a strong light.

B.3 Extinction

During the photometric observations, both scattering and absorption take place, so that the star light is dimmed or partially destroyed by passing through the

atmosphere. Instead of scattering and absorption, another term *extinction* is used for combination. In addition to the usage of extinction, also *a photometric night* or *a photometric sky* should be defined. If the transparency is strongly variable across the sky and/or variable in time then the sky is not photometric.

When doing photometry, it is convenient to assume the atmosphere as a plane parallel layer which is uniform in opacity both vertically and horizontally. This is so called *Slab Model.* Thickness of the slab measured vertically from the observer on the ground to the top edge of the slab is defined as *one air mass.* The zenith distance of an object in the sky is an angle between the observer's zenith and a line connecting the object with the observer where it is shown on figure B.1 as z. This is given as the secant approximation of the air mass;

$$X = \sec z \tag{B.5}$$

Using the equatorial coordinate system, it is easy to calculate the value of $\sec z$, for any object in the sky.

$$X = \sec z = (\sin\phi \sin\delta + \cos\phi \cos\delta \cos h)^{-1} \tag{B.6}$$

where ϕ is the observer's geographic latitude, δ is the object declination, and h is the object hour angle ('–' for east of the Greenwich, '+' for west of the Greenwich).

At large values of z, this approximation does not work well. Bemporad (1904), considered curvature, density of the atmosphere and atmospheric refraction, then obtained a more realistic model. Hardie (1962) used this model and derived an interpolation formula

$$X = \sec z - A(\sec z - 1) - B(\sec z - 1)^2 - C(\sec z - 1)^3 \tag{B.7}$$

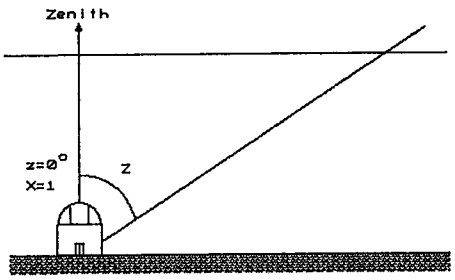

Figure B.1. Slab Model of the Earth's Atmosphere

where

$$A = 0.0018167$$

$$B = 0.0028750$$

$$C = 0.0008083$$

and z is the apparent zenith distance.

Since the physical process of absorption acts to absorb a certain fraction of the incident light, difference between magnitude of the incident light, m_o (before entering to the atmosphere), and the magnitude of the light reaching the detector, m (after passing through the atmosphere) is directly proportional to the air mass X.

$$m_o - m \propto -X$$

$$m_o = m - \mathrm{k}X$$

$$m_o = m - \mathrm{k}_\lambda X \tag{B.8}$$

where k, X are always positive.

When the spectral response defined by each filter is so broad and is not monochromatic, some difficulties arises even you can estimate k_λ from the graph of the

k versus λ on a given night at an observing site. This situation can be eliminated by averaging the curve over the wavelength interval of the filter's spectral response. But another complication comes from the star lights; different stars have different colors. Thus, on the same night and with the same filter, stars of different colors will undergo different amounts of atmospheric extinction (relatively, hotter stars have more).

This situation is handled by introducing another extinction coefficient. For a certain spectral response λ, k_λ will be

$$k_\lambda = k'_\lambda + k''_\lambda \, (B - V) \tag{B.9}$$

where k_λ is the extinction coefficient for the spectral response λ, k'_λ is the principal extinction coefficient, k''_λ is the color dependent extinction coefficient, and $(B - V)$ is the difference between blue and visual magnitudes in UBV photometric system. In the UBV system $(B - V) = 0$, when the star's spectral type is A0 which is not effected by the interstellar absorption. Then combining equation B.8 with the equation B.9 we get

$$m_o = m - k'_\lambda \, X + k''_\lambda \, X \, (B - V) \tag{B.10}$$

Hardie (1962) explains k'' for each spectral response in a given photometric system, besides k'' coefficients can be approximated easily;

1. Visual: $k''_v = 0^m.00 \pm 0^m.01$

2. Blue: $k''_b = -0^m.03 \pm 0^m.01$

3. Ultraviolet: k''_u depends on the star's spectral type and luminosity class, and amount of the interstellar extinction where it is effected. So, an exact approximation can not be done for this spectral response. In practice however, a bad assumption can be done by equaling $k''_u = k''_b$.

In *ubvy* photometric system however, since spectral responses are small compared to UBV system (table B.1), k'' coefficients are so small, so that they can be omitted. In red and infrared photometry they can be omitted also.

B.4 Observation Methods

To measure light one must somehow catch and register it. Four main types of light receptors have been widely used in astronomy: *visual, photographic, photoelectric, and charge coupled device (CCD).* Here, only photoelectric photometry will be dealt basically for the completeness of the observations explained in section 2.3.

For the photoelectric effect, a certain amount of light (number of photons per second) releases a certain amount of electrons; n times as much light releases, precisely, n times as many electrons. The problem of comparing star brightness in visual and photographic photometry, is thus reduced to the problem of measuring and comparing electric currents, which can be done more accurately. Theoretically, accuracies of better than ten-thousandth of a magnitude should easily be attainable for brighter stars. But in practice the atmosphere sets extreme limits of several kinds to precisions of about $\pm$ 0.01 magnitude for short single readings.

There are two kinds of photometry, depending on extinction. *Absolute photometry* relies on knowledge or assumption of extinction coefficients and reduces each observation separately for extinction. *Differential photometry,* relies strictly on comparison of a variable with one or more immediately adjacent comparison stars known not to be variable. If a comparison star is close enough in position and color, and if readings on it are taken often enough, presumably any atmospheric effects on the variable are nearly identical to those on the comparison; hence a simple running

difference of their magnitudes eliminates all first-order extinction coefficients effects.

As a result, practically, the amount of light coming from the star is not measured absolutely, rather, the unknown is compared with several stars of similar brightness whose magnitudes are already well established in a standard sequence:

$$m = -2.5\log(d/f) \tag{B.11}$$

$$\Delta m = m_* - m_s \tag{B.12}$$

where Δm is called the raw instrumental differential magnitude computed at the time of $*$ deflection, m_s is the magnitude of reference star (standard), m_* is the magnitude of another star, measured with respect to m_s, d is the measured deflection in response to the light and f is the gain of whole amplifing system. Combining equation B.12 with B.10 we get

$$\Delta m_o = \Delta m - \mathrm{k}'_\lambda \, \Delta \, X - \mathrm{k}''_\lambda \, \overline{X} \, \Delta(B-V) \tag{B.13}$$

where $\Delta X = X_* - X_s$ and $\overline{X} = 0.5(X_* + X_s)$. If we add the photometric system to equation B.13, we would obtain differential magnitudes for the specified filter(s);

$$\Delta v_o = \Delta v - \mathrm{k}'_\mathrm{v} \, \Delta \, X - \mathrm{k}''_\mathrm{v} \, \overline{X} \, \Delta(B-V) \tag{B.14}$$

$$\Delta b_o = \Delta b - \mathrm{k}'_\mathrm{b} \, \Delta \, X - \mathrm{k}''_\mathrm{b} \, \overline{X} \, \Delta(B-V) \tag{B.15}$$

$$\Delta u_o = \Delta u - \mathrm{k}'_\mathrm{u} \, \Delta \, X - \mathrm{k}''_\mathrm{u} \, \overline{X} \, \Delta(U-B) \tag{B.16}$$

And equations B.2, B.3, and B.4 can be written by applying star minus reference to all the filters;

$$\Delta V = \Delta v_o + \psi_v + \Delta(B-V) \tag{B.17}$$

$$\Delta B = \Delta b_o + \psi_b + \Delta(B-V) \tag{B.18}$$

$$\Delta U = \Delta u_o + \psi_u + \Delta(U-B) \tag{B.19}$$

Finally to find the transformation coefficients one must insert equations B.14, B.15, and B.16 to B.17, B.18, and B.19:

$$\Delta V = \Delta v - k'_v \Delta X - k''_v \overline{X} \Delta(B-V) + \psi_v \Delta(B-V) \quad \text{(B.20)}$$

$$\Delta B = \Delta b - k'_b \Delta X - k''_b \overline{X} \Delta(B-V) + \psi_b \Delta(B-V) \quad \text{(B.21)}$$

$$\Delta U = \Delta u - k'_u \Delta X - k''_u \overline{X} \Delta(U-B) + \psi_u \Delta(B-V) \quad \text{(B.22)}$$

Here Δ means reference standard star minus a standard star in a group of standard stars. Rearranging the above equations:

$$\Delta V - \Delta v + k'_v \Delta X + k''_v \overline{X} \Delta(B-V) = \psi_v \Delta(B-V) \quad \text{(B.23)}$$

$$\Delta B - \Delta b + k'_b \Delta X + k''_b \overline{X} \Delta(B-V) = \psi_b \Delta(B-V) \quad \text{(B.24)}$$

$$\Delta U - \Delta u + k'_u \Delta X + k''_u \overline{X} \Delta(U-B) = \psi_u \Delta(B-V) \quad \text{(B.25)}$$

Thus, the plot of the left hand side of equations B.23, B.24 and B.25 with right hand sides will give the transformation coefficients as the slope of the graph or if you have a single pair star measurements, again by solving the same equations for the coefficients you can obtain the same result.

APPENDIX C

OBSERVATIONS OF CLUSTERS

The observations of the clusters NGC2632, Mel 111 and NGC6633 is listed below. Definition of the columns are as follows:

- # is the assigned number,
- m_V is the standard magnitude of the star taken from the reference,
- B-V is the color index taken also from the reference,
- time is taken in UT,
- d_v is the observed deflections in v filter,
- d_b is the observed deflections in b filter,
- Δd_v is the reading errors of the deflections in v filter,
- Δd_b is the reading errors of the deflections in b filter,
- Δbg is the background noise of the photometric system (dark current).

Table C.1. Observations of NGC 2632

Date	#	m_V	B-V	Time(UT)	d_v	Δd_v	d_b	Δd_b	Δbg
02/05/92	17	6.30	0.17	18: 3:55	75.4	7.5	34.5	4.5	3.2
	20	6.78	0.17	19: 4: 4	93.5	8.5	40.9	6.4	6.5
	19	6.85	0.20	19:14: 3	80.2	7.0	34.0	5.0	6.8
	8	7.32	0.19	19:27:42	50.0	6.0	21.0	5.0	5.7
	9	7.54	0.25	19:41:37	38.4	6.7	15.2	6.0	5.5
	12	7.54	0.16	19:50: 2	38.4	7.5	17.0	5.5	5.7
	14	7.70	0.20	19:59:42	32.5	7.4	12.5	6.0	6.5
	16	8.02	0.19	20: 9:56	23.0	6.0	8.0	4.5	5.2

Table C.2. Observations of Mel 111

Date	#	m_V	B-V	Time(UT)	d_v	Δd_v	d_b	Δd_b	Δbg
29/05/92	11	4.99	0.08	20:19:50	102.6	5.5	49.2	2.0	1.5
	9	6.40	0.27	20:31:43	132.9	7.5	55.0	6.2	7.5
	13	6.53	0.18	20:42:50	119.1	9.1	50.5	6.5	5.4
	14	6.63	0.22	20:53:42	106.4	6.0	45.7	5.5	5.2
	7	6.72	0.24	21: 3:19	95.2	7.6	39.3	4.7	5.5
	12	6.73	0.16	21:11:15	98.2	6.9	41.9	6.0	6.0
25/06/92	11	4.99	0.08	19:43: 0	85.5	5.8	38.8	3.6	1.0
	9	6.40	0.27	19:52:55	111.0	8.5	42.6	7.4	7.0
	13	6.53	0.18	20: 3:30	95.0	8.8	36.7	6.1	6.6
	14	6.63	0.22	20:12: 0	85.5	8.5	31.0	5.5	6.7
	7	6.72	0.24	20:22:33	70.5	9.0	26.8	6.0	6.8
	12	6.73	0.16	20:31:15	72.3	7.5	28.2	5.4	7.1

Table C.3. Observations of NGC6633

Date	#	m_V	B-V	Time(UT)	d_v	Δd_v	d_b	Δd_b	Δbg
07/07/92	31	8.77	0.22	21:24:22	18.0	6.5	8.2	5.0	4.5
	32	7.57	0.09	21:31:23	57.5	7.0	27.0	5.2	4.5
	33	8.26	0.24	21:38:24	27.5	5.0	10.4	5.4	4.1
	56	8.21	0.82	21:46:30	32.0	5.7	9.8	6.0	5.0
	66	8.18	0.03	21:53:21	33.0	6.7	18.3	7.0	6.5
	31	8.77	0.22	22:11:35	18.2	6.5	7.0	6.0	5.7
	32	7.57	0.09	22:15:18	55.2	6.5	25.2	6.0	5.5
	33	8.26	0.24	22:19:37	28.2	5.1	12.2	5.0	4.0
	56	8.21	0.82	22:23:58	27.8	5.5	8.0	5.2	5.0
	66	8.18	0.03	22:28: 5	30.4	6.2	16.2	5.0	4.7
24/07/92	31	8.77	0.22	20:57:30	13.6	4.5	5.2	4.6	4.5
	32	7.57	0.09	21: 1:18	41.5	5.0	17.7	5.5	4.3
	33	8.26	0.24	21: 7:10	21.3	4.9	7.5	5.0	4.7
	56	8.21	0.82	21:13:42	22.2	5.2	5.0	5.2	4.0
	66	8.18	0.03	21:17:51	23.0	5.0	10.2	5.0	4.7
	31	8.77	0.22	21:24:36	13.2	5.4	5.2	5.0	4.2
	32	7.57	0.09	21:28:58	41.5	6.0	17.7	5.2	5.0
	33	8.26	0.24	21:36:10	19.2	5.2	7.2	5.7	4.2
	56	8.21	0.82	21:41: 3	20.3	6.2	5.5	5.2	3.2
	66	8.18	0.03	21:45:14	21.0	4.7	10.0	4.7	4.7
	31	8.77	0.22	21:53: 9	11.5	4.7	4.5	5.7	4.0
	32	7.57	0.09	21:56:52	33.0	4.2	13.0	5.2	4.6
	33	8.26	0.24	21: 2:16	16.6	4.7	5.5	4.2	4.0
	56	8.21	0.82	21: 8:12	19.0	4.5	4.5	4.0	4.7
	66	8.18	0.03	22:12:43	18.7	4.1	7.7	4.3	4.2

Table C.3. (cont'd).

Date	#	m_V	B-V	Time(UT)	d_v	Δd_v	d_b	Δd_b	Δbg
31/07/92	31	8.77	0.22	19:30: 8	15.5	5.5	7.0	5.0	4.6
	32	7.57	0.09	19:35:47	50.4	7.2	22.7	5.1	4.1
	33	8.26	0.24	19:42: 4	25.4	6.5	11.0	5.0	4.4
	56	8.21	0.82	19:48:47	27.0	6.7	6.5	6.5	5.0
	66	8.18	0.03	19:53:49	27.5	5.5	11.8	5.7	4.5
	31	8.77	0.22	20:14: 2	15.6	6.0	5.0	6.0	6.0
	32	7.57	0.09	20:19:12	47.2	6.5	19.8	5.5	5.4
	33	8.26	0.24	20:24:53	24.2	5.0	8.6	5.0	4.5
	56	8.21	0.82	20:30:39	24.5	5.5	5.2	6.0	5.0
	66	8.18	0.03	20:37: 2	27.0	6.4	12.0	5.2	4.9
	31	8.77	0.22	20:43:58	13.2	5.7	6.0	5.0	4.9
	32	7.57	0.09	20:49: 2	44.4	5.5	9.2	6.0	7.0
	33	8.26	0.24	20:54:45	22.6	5.5	8.8	5.7	4.3
	56	8.21	0.82	21: 0:24	24.2	5.5	5.7	5.2	5.0
	66	8.18	0.03	21: 6:19	25.2	7.0	11.5	5.0	4.9
	31	8.77	0.22	21:13: 0	14.0	4.7	7.0	4.5	4.0
	32	7.57	0.09	21:17:27	45.3	5.2	21.0	4.7	4.1
	33	8.26	0.24	21:22:41	22.5	4.6	9.5	4.6	4.5
	56	8.21	0.82	21:28:24	23.7	4.2	6.4	5.0	4.0
	66	8.18	0.03	21:33:14	25.8	5.5	12.0	5.2	5.2
	31	8.77	0.22	21:41:12	13.7	4.5	6.4	4.9	4.0
	32	7.57	0.09	21:44:49	43.0	5.2	19.6	5.0	4.5
	33	8.26	0.24	21:48:38	22.2	4.5	9.9	5.0	4.5
	56	8.21	0.82	21:52:19	23.0	4.2	6.0	4.2	4.0
	66	8.18	0.03	21:55:59	23.5	4.8	11.2	4.8	5.2

Table C.3. (cont'd).

Date	#	m_V	B-V	Time(UT)	d_v	Δd_v	d_b	Δd_b	Δbg
02/08/92	31	8.77	0.22	19:52: 5	17.2	5.7	7.8	5.0	4.8
	32	7.57	0.09	19:56:38	53.8	5.9	23.2	4.9	5.0
	33	8.26	0.24	20: 1: 7	28.0	5.0	10.6	5.0	4.6
	56	8.21	0.82	20: 5:39	28.7	6.4	6.5	5.5	3.2
	66	8.18	0.03	20:11:12	30.2	5.2	14.0	5.0	5.0
	31	8.77	0.22	20:16:46	15.8	5.5	7.2	4.9	4.9
	32	7.57	0.09	20:20:57	54.0	5.8	26.8	6.0	4.8
	33	8.26	0.24	20:26:31	27.8	5.8	11.7	5.2	5.0
	56	8.21	0.82	20:30:42	28.5	5.0	7.8	4.9	4.5
	66	8.18	0.03	20:35:35	28.8	5.2	14.0	5.0	4.8
	31	8.77	0.22	20:42:20	16.3	5.0	7.8	5.5	5.0
	32	7.57	0.09	20:46:21	51.2	6.0	24.0	5.2	6.0
	33	8.26	0.24	20:50:55	28.0	5.0	11.5	5.0	5.0
	56	8.21	0.82	20:55:20	27.2	4.8	7.0	5.5	4.8
	66	8.18	0.03	20:59:53	28.9	5.0	13.0	6.0	4.8
	31	8.77	0.22	21: 5:42	14.0	5.0	5.5	5.0	5.0
	32	7.57	0.09	21:10: 0	51.0	6.0	21.6	5.5	5.5
	33	8.26	0.24	21:14:28	27.3	5.9	10.0	4.9	4.6
	56	8.21	0.82	21:18:47	27.6	6.0	7.0	5.5	5.4
	66	8.18	0.03	21:22:47	27.0	5.5	13.0	5.8	5.2
	31	8.77	0.22	21:30: 5	15.5	5.5	6.4	5.5	5.5
	32	7.57	0.09	21:34:41	50.8	5.8	23.2	6.2	4.2
	33	8.26	0.24	21:39: 9	26.6	5.0	10.2	4.8	4.5
	56	8.21	0.82	21:43:39	27.0	4.9	7.0	4.5	4.0
	66	8.18	0.03	21:48: 3	27.6	4.3	12.2	4.5	4.0

APPENDIX D

BASIC PRINCIPLES OF SEMICONDUCTORS AND CCD

When impurity atoms are added to the semiconductor, its conductivity is increased. This addition to the semiconductor is called *doping*. If the impurity atom has more valance electrons than the semiconductor, then it will donate these negative charges to the conduction band (n type). Conversely, if the impurity atoms have fewer valance electrons than the semiconductor then a positively charged hole is left in the valance band ready to accept any available electrons (p type).

When a p-n junction is formed, a narrow region forms on either side of the junction in which the majority charge carriers are *depleted* relative to the their concentrations well away from the junction.

If a positive voltage is applied to the p side of the junction it will tend to reduce the built-in potential barrier and attract more electrons across the junction, whereas a negative voltage, will improve the internal barrier and increase the depletion region. Therefore, on one-side of a p-n junction there is a region which is more negative and on the other side there is region which is more positive then elsewhere in the crystal.

Thus, if an array of pixels (i.e picture elements, formed from p-n junction), where each pixel has the ability to absorb photons, is constructed then each pixel can produce electrons and holes in the semiconductor by using the energy gathered from the photons. Electron-hole pair is then separated apart by the potential difference across the junction, before they can recombine. Storing of successive electrons, accumulating on the same pixel, can be maintained by using capacitor logic in the semiconductor silicon size (0.1 μm). Electrons are drawn to the region of greatest positive potential buried in the n type layer which therefore behaves like a capacitor (MOS*Metal-Oxide*

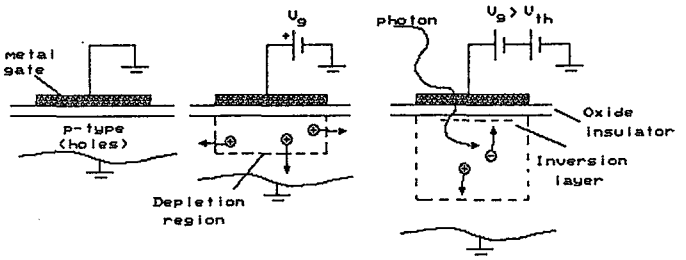

Figure D.1. A single MOS storage pixel, the basic element in a CCD

Semiconductor structure). The MOS capacitor is the combination of two parallel plate capacitors, the oxide capacitor and the silicon depletion region capacitor. Therefore the capacitance is proportional to the area of the plates and inversely proportional to their separation. The depletion width can also be controlled by controlling the voltage on the plate. This means that the capacity to store charge can also be controlled. As the voltage on the plate increase, the 'depth' of the depletion region increase. Then, at a certain threshold voltage, electrons (for a p type semiconductor) will be drawn to the plate (figure D.1) (Boyle and Smith, 1971).

After storing charges, they must be collected and counted. This is done by constructing structures on the CCD, known as three-phase which is commonly used one. Semiconductor silicon is covered with a thin insulating layer made from silicon oxide. On top of these, three sets of metal plate strips are placed. In each column of these strips, there is a column insulator to form an array (figure D.2). One of the three strips is set to a more positive voltage than the other two, so that the depletion region is formed under this strip. By heavily doping silicon crystal structure with a certain impurity atoms, it is possible to prevent any movement of charge along the length of

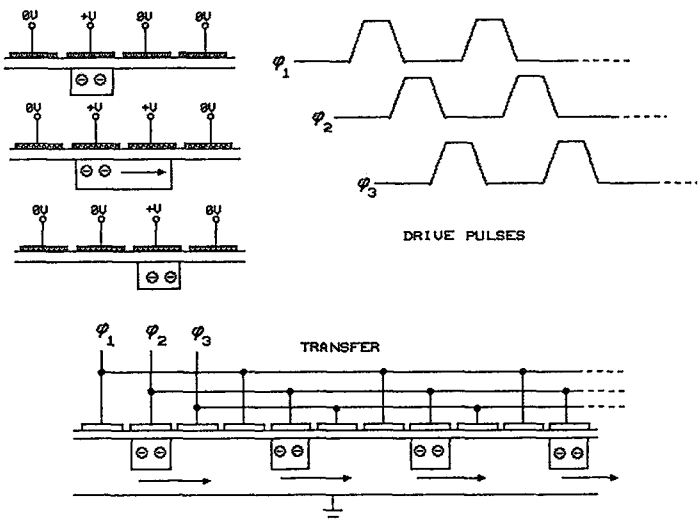

Figure D.2. Charge Coupling and timing waveforms in a three-phase CCD

the plate. These channel stops and three strips defines the basic picture element of the CCD (pixel).

To transfer charge (charge-coupling) from under one plate to the area below an adjacent plate, the voltage on the adjacent plate must be raised to the same value as the first one. Then the charges will be shared depletion regions of these two plates. Then lowering the original plate voltage will collect all the electrons to the adjacent plate. Thus to transfer the charge one pixel one must do this raising and lowering process three times. Remember that this shift is done for a column. To transfer the left most column this procedure must be applied number of rows times. By constructing a simple timing diagram, electronically, all the transfer can be finished successfully (figure D.2) (Boyle and Smith, 1971).

Buried Channel CCD

In surface-channel CCD's the most positive potential lies at the silicon

surface immediately under the insulating oxide layer. Therefore, electrons are stored and transferred at the surface of the silicon semiconductor. However in these type of CCD's, the surface layer has crystal irregularities and defects in the lattice structure. This will cause the electrons to be trapped but not released.

To overcome this inability, another silicon layer put onto the existing p-type substrate to separate it from Si-SiO_2 interface. If the layer is chosen to be n-type, a depletion region is created with a collecting layer which is considerably buried inside the bulk silicon. This kind of CCD's are called *buried-channel* CCD's (McLean, 1989).

Although the electrons now can be released in buried channel CCD's, the storage capacity is reduced, i.e. a buried-channel CCD will saturate before an equivalent surface-channel CCD.

Backside-illuminated CCD

To have electrons at the depletion region, photon flux should fall on the plates. However this usual configuration of CCD would give us a spectrum with absorption of blue light.

This problem is solved with exposing the CCD from backside. And also thick silicon substrate must be reduced in thickness. Then it can have required response spectrum. This modification, however makes the chip more fragile for warping (McLean, 1989).

D.1 Dark Current in CCD's

At room temperature, in the silicon lattice structure, random mechanical motion of atoms can release energy to liberate electron-hole pairs in the absence of light. This can be *dark current* for a CCD. It is important, if we think that the typical

dark current of a CCD is about 10^5 electrons per second per pixel. This much of current is enough to saturate the image in seconds. Thus without preventing dark current, a CCD is useless for astronomical purposes, but can be used with a fast timing of the order of 5MHz for clearing the CCD before every image.

For CCD, there are three main dark current sources:

1. thermal generation and diffusion in bulk silicon
2. thermal generation in the depletion region
3. thermal generation due to surface states at the junction between Si and SiO_2 insulation layer

The dominant source of dark current comes from the surface states (McLean, 1989).

The easiest way to overcome the dark current is to cool the CCD with liquid nitrogen (LN_2) or liquid helium. In silicon the dark current decreases at a rate of 10^oC per one-third of previous current value.

To get a considerable cooling on the CCD, the chip should be in mechanical contact with a good heat conductor where it is connected to a bath of liquid nitrogen or helium. To prevent frosting the whole configuration is built into the vacum chamber, leaving an optical window for observations. Such chambers are called *cryostat.*

Dark current can also be reduced by operating the CCD in inversion mode (Mackay, 1986). In this mode plate voltage is kept near zero volts, rather than +10V. And the clock level applied to other plates are set to -10V. With this configuration, holes are attracted up to the Si-SiO_2 interface layer at these plates thus populating the problematic states with holes. This mode of operation also eliminates problem of charge capture and residual images appeared in saturations.

D.2 Physical Disturbances Effecting the Image

High energy subatomic particles entering the Earth's atmosphere from outer space will generate a shower of secondary particles, which can be stopped by a thick layer of silicon. The energy generation due to this cosmic rays is around 80 electrons per pixel per micron of thickness of silicon. Thinned backside-illuminated CCDs are therefore less effected than thicker frontside illuminated CCDs.

There is no single way to eliminate this problem due to random generation of cosmic rays. The practical way is to eliminate them from the image after the exposure is taken. If the region is crowded and taking object images then the only chance to remove them is to make multiple images and compare.

Another physical effect is the luminescence. An electrical path in the semiconductor can act like a light-emitting-diode (LED). This problem can be seen also when an incorrect voltage is applied to the device.

D.3 Bad Pixels and Charge Transfer Efficiency (CTE)

When transferring the collected electrons, there may be problems if the adjacent depletion regions are

- virtually empty
- almost full
- if it is a defective pixel

When the depletion regions of one column is completely full (saturation), you may have the problem of charge spilling by the spread of electrons to adjacent pixels. If the

saturation is strong enough then you may have whole the column filled with electrons. This can happen if a single source is over exposed in the image (McLean, 1989).

Charge transfer efficiency (CTE) is defined for trapped electrons during the transfer. Having poor CTE causes tails on columns of the image. These trapped electrons are not lost in depletion regions whereas they are skimmed to be released later. This concept is related to *deferred charge*. Deferred charge can be due to design faults which results in potentials at certain locations and charge traps due to impurities. To overcome such poor CTE effects simplest thing to do is to illuminate the whole CCD with a soft light source, so that all the depletion regions will have a certain amount of electrons before each exposure. By doing this the background level is raised by about 100 electrons. This procedure of adding an amount to the signal is attributed as *'fat zero'* (Mackay, 1986).

D.4 Noise Sources and Calibration of CCD

Since CCD can detect light levels of just a few tens of electrons (corresponding to voltage changes of a few tens of μVs), if the design of the CCD was not careful enough, such signal will be discarded by other causes of voltage variations.

The main noise comes during the transfer of the electrons from one pixel to the adjacent pixel. When the transfer of electrons is not %100, then a portion of electrons remain in the depletion region of the pixel, which will be used by the successive transfer. The term *readout noise* is used to define this effect.

Thus noise produced by a signal-processing chain, which converts number of electrons to DNs (data numbers), must be reduced to a minimum, to have a minimum total noise originating only from CCD chip. The main sources of noise originating from

CCD can be listed as follows:

- background charge associated with fat zero offsets
- transfer loss fluctuations
- reset noise
- MOSFET noise
- fast interface noise

Calibration of the CCD can be managed by obtaining the readout noise or calibrating it exactly. Calibration of the readout noise should be done with independent measurements of the properties of various components of the signal-processing chain (White et. al, 1974).

The method for calculating the readout noise and as well as gain of the system is explained below: (characteristics of the CCD, calculated from this method will be a function of the optical system producing the images, filters which are used, and the gain settings of the CCD digitizer) (Tyson, 1986)

1. Enough number of flat-field images must be taken. A *flat-field* image is obtained by taking the image of an approximately uniform illumination of a white surface. Also the optical system must be focused to infinity and the power supply for the light source should be stable enough during the exposures of flat-field images.

2. Set the desired gain settings of the digitizer. By this setting, the bias level should be below 20 ADU (Analog-Digital Unit). The bias level is defined as the mean pixel value on the CCD in the absence of light for a zero integration time. Practically however, it can be obtained from a dark frame at a short exposure. By adjusting offset setting, the mean can be arranged about 20-30 ADU.

3. Now take a couple of images for different exposure times. Minimum of four exposure times are required. For consistency of the light source first exposure time should be repeated at the end of the imaging.

4. From the resultant image, obtain median value of the histogram and measure the standard deviation of the histogram. Since two images are taken the values must be averaged by dividing two.

5. Plotting median values versus integration times should give a linear relation, whereas at integration times if saturation is in effect, then the linearity of the image deviates. This gives a good reference for the highest signal level that the ADU level remained linear with time. This level is also a function of the gain setting of the digitizer.

6. A linear regression on the linear part of the graph will give us true bias level (in ADU) for zero integration time at the y-intercept. This bias level must be subtracted from every image in the future usage. Also, the slope of the graph is referred as the *speed* of the system (in ADU/sec).

7. Then compute the variance for each averaged exposure time. Plot the variance versus bias corrected median signal level. After a linear regression on linear part of the graph, the slope and y-intercept of it will give the system gain g (in ADU/electron) and readout noise R^2 (ADU^2), respectively.

Results of the calibration is summarized below, where n_{med} is the median signal level, t is the exposure time, σ^2 is the variance of median values.

n_{med} vs t	→ slope	speed of the system	ADU/sec
	→ y-intercept	bias level	ADU
σ^2(n) vs n_{med}	→ slope	gain	ADU/electrons
	→ y-intercept	readout noise	ADU^2

Thus the gain and the readout noise of the CCD would be:

system gain	g	ADU/electron
	$p = 1/g$	electron/ADU
readout noise	R	ADU
	$r = R/g$	electrons

D.5 Correcting the Histogram of an Image

Before starting any imaging sequence with the CCD, care should be taken for each setting of the instrumentation. There may be fatal errors, that can not be solved by any other method, where they may arise after the exposures are taken. To have calibrated and well defined images, histogram of the images are the best way of detecting any faulty in the image.

Histogram of an image is obtained by counting the number of electrons, accumulating at each ADU level. ADU level is between 0 and 255 for 8-bit sampling. Thus, theoretically, dark current should fall into lowest ADU level. However, as the exposure time increases, dark current also increases. So, the simplest correction for the histogram is to subtract the dark frame from the original frame. To do this, after and/or before the imaging sequence, a dark frame should be taken *'with the same exposure time'* as the imaging sequence is done. This subtraction is very important for long exposures. Since all ADU levels are pulled toward zero, saturation of the objects are also prevented.

After a dark subtraction, flat-field correction should be done to normalize the whole frame. This correction also smooths the background, which gives more accurate sky values and error calculations.

Now, the image frame is ready to determine the proper values of the exposure time, gain and offset settings. A sample manipulation is shown in figure D.3. Top

panel is the original frame, middle one is after the dark subtraction, and the bottom one is after the flat-field correction, applied to the middle image. Histogram of the image is shown for each image.

D.6 Photometry with CCD

In general, the accuracy of the brightness obtained from a CCD image is very high. Calibration of CCD systems against the photomultiplier tube systems to high accuracy is very difficult due to the mismatch between the working principles of both systems. However since CCDs perform better and can be calibrated easily, everything done for a photomultiplier tube should also be done for a CCD also. In other words, methods for calibration, standardization, data manipulation procedures must be constructed for CCD also (Tyson, 1986 and McLean, 1989).

There are two basic procedures for obtaining photometric data from CCD images:

1. *Aperture Photometry*: After the CCD image has been obtained, a computer program is used to reconstruct the signal which would have been obtained from an object in the field of view if the light had passed through a physical aperture (usually circular). This imaginary aperture is called a *software aperture*. Estimation of the background level, the center of the optical image, and the shape of the image itself are very important parameters of the method.

2. *Profile Fitting*: Also called *point-spread-function* (PSF) fitting. This method relies on the modelling the image rather than summing over the image. Mathematical curves are fitted to the real data until a good match is obtained.

The use of CCDs for photometric measurements is founded on two basic

assumptions:

- The response of each pixel is a well-defined function of exposure level, optical bandpass, and CCD architecture and control.
- The incident signal from the astronomical source can be calibrated or transferred to the desired *standard* system.

An understanding of the image profile and the centroid of the image is important since centering errors and inappropriate apertures or fitting parameters can lead to systematic effects. Some more important items are as follows:

- Passband mismatch of the filters.
- Red/infrared leaks in the filters which complicates flat-fielding.
- The finite opening and closing times of electromechanical shutters.
- Changes in the airmass for long on-chip CCD integrations.

The first and second items can be eliminated at the design section.

Before starting a photometric procedure, bias subtraction, dark subtraction and flat-fielding should be applied correctly. Extreme care and patience at the telescope is required to ensure that all necessary calibration data are obtained with very high accuracy not to limit the photometric determinations, and that nothing happened on that night, which might make reductions difficult.

Once photometric values are obtained they must be compared or calibrated against well-measured *standard* sources. Photoelectric standard stars must be observed over a wide range of airmasses and cover an suitable range of spectral types to obtain

color coefficients. Then the instrumental magnitudes are calculated from

$$m_{raw} = -2.5\log(n) \tag{D.1}$$

where n is the counts read from CCD in electrons/sec. Then these magnitudes can be compared with the standard stars to produce the transformation. For the transformation the following parameters should be calculated:

1. *Zeropoint*: the magnitude corresponding to 1 count/sec for a star of zero color-term above the atmosphere.

2. *Color equation*: This is the relation between CCD photometric system and older photoelectric system.

3. *Extinction factor*: Light-loss per unit airmass through the atmosphere.

Thus resulting equation for the apparent magnitude will be

$$m = -2.5\log -\alpha X + \beta CI + ZP \tag{D.2}$$

where α is the coefficient for airmass (equivalent to k'_λ), β is the color coefficient (equivalent to k''_λ), X is the airmass, CI is the appropriate color index, ZP is the zero point for the transformation.

For long exposures the airmass can be approximated by the following equation:

$$\overline{X} = \frac{X_0 + 4X_{1/2} + X_1}{6} + O(e) \tag{D.3}$$

where X_0 and X_1 are the airmasses at start and end times of the exposure respectively, $X_{1/2}$ is the airmass at middle of the exposure, $O(e)$ is a small error of about 1 part in 1000.

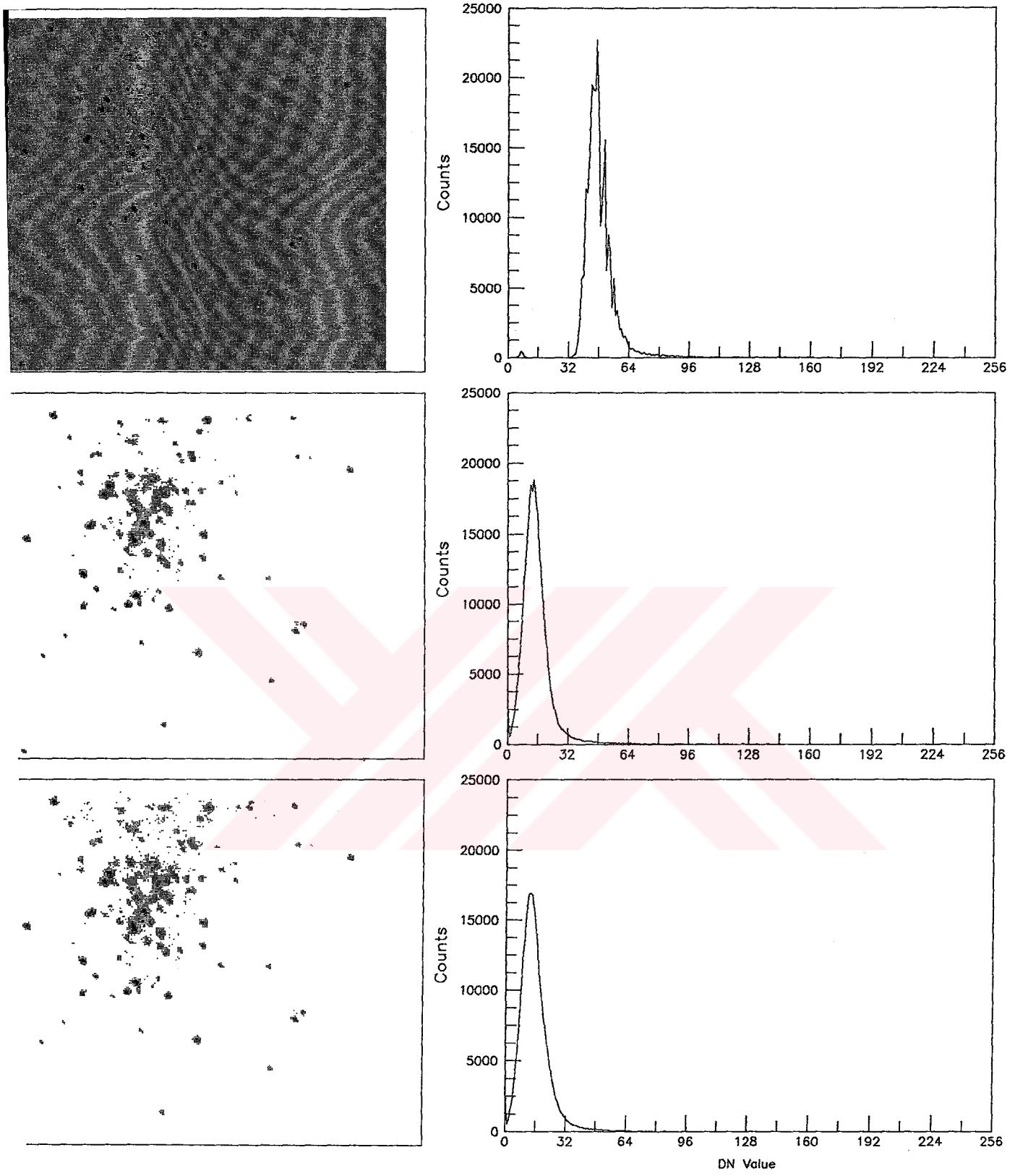

Figure D.3. A sample image of M13: Original one (top), after dark subtraction (middle), after flat-field correction (bottom)